P-06-137

Oskarshamn site investigation

Detailed ground geophysics at Laxemar, autumn/winter 2005/2006

Magnetic total field and resistivity

Hans Thunehed, Carl-Axel Triumf
GeoVista AB

October 2006

Svensk Kärnbränslehantering AB
Swedish Nuclear Fuel
and Waste Management Co
Box 5864
SE-102 40 Stockholm Sweden
Tel 08-459 84 00
+46 8 459 84 00
Fax 08-661 57 19
+46 8 661 57 19

ISSN 1651-4416
SKB P-06-137

Oskarshamn site investigation

Detailed ground geophysics at Laxemar, autumn/winter 2005/2006

Magnetic total field and resistivity

Hans Thunehed, Carl-Axel Triumf
GeoVista AB

October 2006

Keywords: Laxemar, Ground geophysics, Magnetic total field, Magnetisation, Resistivity, Lineament, Deformation, NS001, NS059, EW007, NE138A, NS046A, NW932C, Soil cover thickness.

Abstract

Detailed geophysical measurements have been performed in the Laxemar area. A total of approximately 3.45 km^2 were covered with measurements of the total magnetic field. The survey area borders to a previous magnetometry survey perfomed at Laxemar and a mosaic map of the survey results has been produced. Three areas, 400 by 400 m each, were covered with resistivity measurements with the ABEM Lund imaging system.

The measurements of the magnetic total field were carried out along profiles directed in north-south, with a profile spacing of 10 m and a station separation of 5 m. A number of low-magnetic semi-linear features appear in the results. The most prominent of these correspond to known deformation zones like e.g. NS001, NS059, EW900 and NW042 of which some have been modelled to reflect the dip and geometric complexity of the source. A number of new short lineaments have been possible to identify in the presented data. Some of the lineaments identified in earlier activities have been re-evaluated. Rock with rather high magnetization appears in the survey area in a band trending WNW-ESE. The corresponding magnetic pattern is rather irregular although banding occurs locally at some places.

Resistivity measurements with the ABEM Lund Imaging system were carried out along east-west oriented profiles separated by 10 m. The electrode separation was 5 m and a total of 81 electrodes per line were used. Measurements were performed with a gradient array protocol resulting in a depth of investigation of up to 60 m. The three survey areas were located around the north-south trending lineaments NS046, NS059 and NS001 respectively. The formerly identified lineament NS046 appears as a quite weak resistivity anomaly not even detectable at all profiles. NS059 shows a rather complex character. The zone itself does not produce a particularly strong anomaly, but within the investigated volume it is associated with a rather wide zone of low bulk resistivity. The inferred deformation zone NS059 is interpreted to dip towards west based on the character of the resistivity anomaly. The inferred deformation zone NS001 appears as a rather distinct resistivity anomaly with high resistivity host rock. Based on the character of the resistivity anomaly NS001 is interpreted to dip towards west.

The soil cover thickness has been estimated from the resistivity measurements. Maps of soil cover thickness and bedrock relief are presented for the three areas.

Sammanfattning

Detaljerade geofysiska mätningar har utförts i Laxemar-området. Totalt cirka 3,45 km^2 har undersökts med mätning av magnetiskt totalfält. Undersökningsområdet gränsar till ett tidigare mätområde för magnetometri i Laxemar och en mosaik av de två undersökningarna har sammanställts. Tre områden, 400 gånger 400 m vardera, har undersökts med resistivitetsmätningar utförda med ABEM Lund imaging system.

Mätningarna av magnetiskt totalfält har utförts längs nord-sydliga profiler separerade med 10 m och med ett mätpunktsavstånd av 5 m. Ett antal lågmagnetiska semi-linjära strukturer kan ses i resultaten. De mest signifikanta av dessa motsvaras av kända deformationszoner som t ex NS001, NS059, EW900 och NW042. Några av dessa deformationszoner och lineament har modellerats för att belysa källans stupning och geometriska komplexitet. Ett antal nya kortare lineament har också varit möjliga att identifiera i data. En del lineament som identifierats i tidigare arbeten har omvärderats. Berggrund med hög magnetisering förekommer i ett WNW-ESE-riktat stråk i området. Det motsvarande magnetiska mönstret är tämligen oregelbundet även om bandning förekommer lokalt.

Resistivitetsmätningar med ABEM Lund Imaging system utfördes längs öst-västliga profiler med 10 m avstånd. Elektrodseparationen var 5 m och totalt 81 elektroder användes på varje profil. Mätningarna utfördes med ett gradientprotokoll resulterande i ett undersökningsdjup av upp till 60 m. De tre undersökningsområdena var lokaliserade kring lineamenten NS046, NS059 respektive NS001. NS046 uppträder som en tämligen svag resistivitetsanomali som inte ens är detekterbar på alla profiler. NS059 uppvisar en relativt komplex karaktär. Själva zonen producerar inte någon speciellt kraftig anomali, men den är associerad med en relativt bred zon med låg bulkresistivitet inom det undersökta området. Deformationszonen NS059 tolkas stupa mot väster baserat på karaktären av resistivitetsanomalin. Den tolkade deformationszonen NS001 uppträder som en distinkt resistivitetsanomali omgiven av högresistivt berg. Karaktären på resistivitetsanomalin indikerar en stupning mot väster för NS001.

Jordtäckets tjocklek har uppskattats från resistivitetsmätningarna. Kartor av uppskattat jorddjup och berggrundstopografi presenteras.

Contents

1 Introduction

This document reports the results gained from the ground geophysical measurements of the magnetic total field and resistivity at Laxemar, autumn 2005, which is one of the activities performed within the site investigation at Oskarshamn. The work was carried out in accordance with the activity plan AP PS 400-05-079. In Table 1-1 controlling documents for performing this activity are listed. Both activity plan and method descriptions are SKB's internal controlling documents.

The ground geophysical measurements were carried out by GeoVista AB during November 2005 to March 2006 at Laxemar in an area covering around 3.45 km^2, Figure 1-1. The survey included measurements of the magnetic total field and resistivity. The resistivity distribution was investigated with the ABEM Lund Imaging System. The processing and interpretation of the data was performed by GeoVista AB and the results are expected to support the future site investigations at Laxemar.

The original results of the survey are stored in the primary data bases (SICADA and GIS) and they are traceable by the activity plan number AP PS 400-05-079.

The grid system over the area was prepared by GeoVista AB.

Table 1-1. Controlling documents for the performance of the activity.

Activity plan	**Number**	**Version**
Detaljerade markgeofysiska mätningar i Laxemar under hösten 2005	AP PS 400-05-079	1.0
Method descriptions	**Number**	**Version**
Metodbeskrivning för markbaserad magnetometri	SKB MD 212.004	1.0
Metodbeskrivning för resistivitetsmätning	SKB MD 212.005	1.0

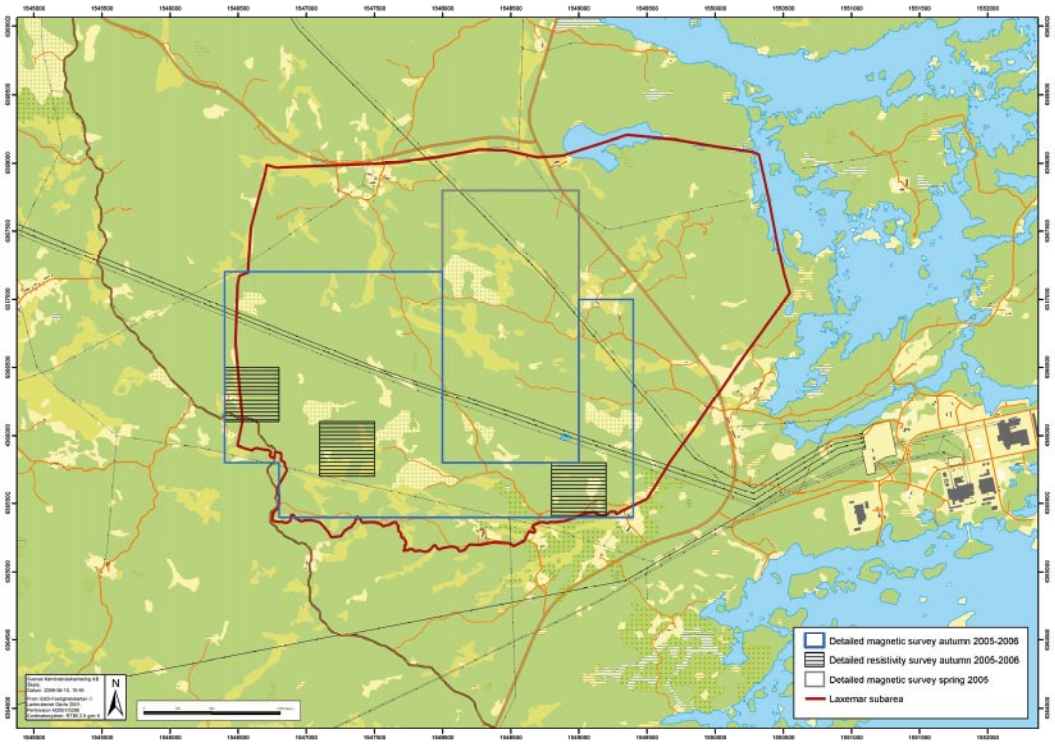

Figure 1-1. *Location of the area at Laxemar where the detailed measurements of the total magnetic field were carried out (blue polygon). The three areas covered by detailed resistivity measurements are shown with black quadrates. The location of the area where detailed measurements of the total magnetic field were carried out in spring 2005 is shown with a grey polygon /8/.*

2 Objective and scope

The results of the detailed ground geophysical survey at Laxemar are expected to support the future site investigations at Laxemar by reflecting the:

- Deformation of the bedrock by possible regional zones, local major zones, local minor zones and general fracturing.
- Lithological homogeneity of the bedrock.

This is done by the processing and interpretation of the collected data of the magnetic total field and resistivity. The magnetic total field reflects the magnetisation of the ground. The magnetisation in the Laxemar area is dependent on the rock type and the alteration and deformation of the rock, which is shown by thorough investigations of the magnetic properties of the area /1, 2, 3, 4, 5/. There is also a clear correlation between fracturing of rocks and the resistivity of rocks /3, 6, 7 and 8/.

3 Equipment

3.1 Description of equipment/interpretation tools

The measurements of the magnetic field were performed with magnetometers Gem Systems GSM-19 of which one was used as a diurnal base station.

The measurements of the resistivity were carried out with an ABEM Lund Imaging System using a distance of 5 m between the electrodes and a gradient configuration, Figure 3-1.

The magnetometers and the resistivity systems used are calibrated at the factory and a quality controlled performance of them is assured by following method descriptions and the internal quality plan of the activity as presented to SKB before the survey started.

The processing, interpretation and reporting included the use of the following software:

Grapher v6 (Golden Software).

Oasis Montaj 5.0 (Geosoft Inc).

RES2DINV version 3.5 (Geotomo Inc).

RES3DINV version 2.1 (Geotomo Inc).

ModelVision Pro 6.0 (Encom Technology).

Profile Analyst 6.0 (Encom Technology).

Mag3D (UBC GIF).

MapInfo Professional 7.5 (MapInfo Corporation).

Discover 7.1 (Encom Technology).

ArcView (Environmental Systems Research Institute Inc.).

Microsoft Excel (Microsoft Corp.).

Microsoft Word (Microsoft Corp.).

Adobe Acrobat and Adobe Distiller (Adobe Systems Inc.).

Figure 3-1. *Measurements of the resistivity with the Lund Imaging System (ABEM AB).*

4 Measurements, processing and interpretation

4.1 General

The detailed geophysical survey at Laxemar consisted of the following main sub-activities:

- preparation of a grid system.
- measurements of the magnetic total field.
- measurements of the resistivity by the use of the ABEM Lund Imaging System with a gradient protocol and an electrode spacing of 5 m.
- processing, interpretation and reporting.

4.2 Preparation of a grid system

By the use of a high resolution GPS (accuracy better than 0.5 m in general) east-west lines were staked all over the area to be measured. Normally the distance between these lines was 100 m though less in some areas. Along these lines, a mark was positioned in the terrain every 20th m.

The distance along the profile for magnetic measurement stations was established with the use of a 1.67 m long stick which was laid out three times to give 5 m advance to a new station. The orientation along the profile was controlled with a compass and the marks every 100 m (see above). Since the survey to a large extent was performed during the winter it was usually also possible to see the walking track along a previous profile 10 m away.

4.3 Measurements

4.3.1 Measurements of the magnetic total field

The magnetic total field survey was conducted with several Gem Systems GSM-19 magnetometers of which one was used as a diurnal base station. One reading at the base station was registered every 10 seconds and was used to make a diurnal correction of the data collected with the mobile magnetometer.

The magnetometers were time synchronized every morning before starting the survey.

Magnetic readings were taken along profiles with a station interval of 5 m; the profile separation was 10 m. The profiles were directed in north-south covering the entire area of 3.45 km^2.

Apart for the same positions used in the previous survey /8/ a new location was used for the diurnal base station magnetometer:

1547633E/6364363N

The difference in background level between the base stations was examined. Readings were taken with 10 seconds intervals for a few hours at two or three of the stations. The averaged readings were entered as datum levels into the magnetometers in such a way that the data from this survey were levelled with the data from a survey during spring 2005 /8/.

The measurements of the magnetic total field were carried out according to the method description (Metodbeskrivning för markbaserad magnetometri, SKB MD 212.004, version 1.0, SKB internal document).

4.3.2 Measurements of the resistivity with ABEM Lund Imaging System

Electric resistivity was measured with the gradient configuration using an ABEM Lund Imaging System with an electrode distance of 5 m and a roll-along cable system of four active cables. Every cable had twenty-one electrode positions. With one overlapping electrode in every cable connection (three connections) the total distance covered with one layout is 400 m.

Resistivity measurements with the Lund Imaging System were carried out along 41 profiles in each of three surveyed areas. The line direction was east-west and the line separation was 10 m.

The measurements of the resistivity with the ABEM Lund Imaging System were carried out according to the method description (Metodbeskrivning för resistivitetsmätning, SKB MD 212.005, version 1.0, SKB internal document)

4.4 Data processing and interpretation

4.4.1 Processing and interpretation of magnetic total field data

The processing performed on the magnetic data was the removal of diurnal variations recorded by the base magnetometer. The data were thereafter added to the data from the survey performed during spring 2005 /8/ to form a mosaic covering most of the Laxemar area. A regular grid with a node spacing of 2.5 m was interpolated to form the base for different map products. The magnetometers were affected by noise close to the major power lines. Corridors around these power lines were therefore blanked out from the grid file.

Based on the grid file, filtering has been carried out in order to produce different types of maps used for the identification of in-homogeneous rock and lineaments. Filtering has included reduction to the pole, vertical derivatives, upward continuation, and horizontal gradients.

The numerical modelling of magnetic data has included voxel based inversion and forward modelling.

Voxel models consist of blocks with rectangular sides that fill up the entire model volume. The magnetic susceptibility of the blocks is iteratively adjusted until a calculated synthetic magnetic anomaly fits the measured data within a specified error limit. The number of blocks in the model will normally exceed the number of measured data. The model must therefore be constrained in order for the process to be stable and converge. Most commonly the model is constrained by smoothness. This will prevent rapid oscillations between neighbouring blocks but will at the same time produce gradual transitions in model properties instead of sharp boundaries. Voxel based inversion has been carried out with the program MAG3D from UBC GIF. Profile Analyst has been used for model visualization.

Forward modelling has been performed over selected magnetic features. The bodies in the models have been assigned magnetic susceptibility values that are compatible with petrophysical data /1, 2, 3/. Model Vision has been used as a modelling tool.

The interpretation of magnetic data has included identification of areas with high magnetization that could indicate the presence of diorite/gabbro or fine-grained dioritoid. In a selection process with the aim to isolate such areas a comparison has been made of the magnetic susceptibility measurements on outcrops, the mapping of diorite/gabbro or fine-grained dioritoids, and the total magnetic field as measured in the detailed ground magnetic survey. The selection of areas with high magnetisation with potential presence of diorite/gabbro or fine-grained dioritoid was based on the following criteria:

- a pronounced magnetic high anomaly is selected if no observations of a magnetic susceptibility in either Ävrö-granite or in the quartz monzodiorite higher than $1{,}500\times10^{-5}$ SI, is found on or very near the anomaly.

The highly magnetized areas have then been compared with the geological map (version 1.2).

An identification of lineaments in magnetic data and a re-evaluation of previously identified lineaments /8/ were also carried out. As explained above the processing of magnetic data by various filters resulted in different types of images of the magnetic field. From such images lineaments were identified. Based on the clearness of the lineament the attribute named "Uncertainty" was given a number of 1, 2 or 3. A low value (1) means that the lineament is clearly identifiable while a high number (3) means that it is less clear.

The identification of lineaments is easier in areas with high magnetic relief. In areas with low and almost uniform magnetisation it is however more difficult to both identify and delineate a lineament. Some of the areas of low magnetisation in the Laxemar area represent parts of local major deformation zones; one example is EW007 that is built up of several such low magnetic areas. In some sections of EW007 the area of low magnetisation may be very thick – up to more than two hundred metres perpendicular to the strike. In such an area it is very difficult to draw a single line that represents the lineament in an appropriate way. If such an extensive area with low magnetisation is found at the crossing with another low magnetic zone with another strike direction, probably representing another possible deformation zone, it becomes even more difficult to draw representative lines. It is problematic in the same product to present, both short lineaments with high degree of spatial significance, together with long lineaments bearing the problem with low spatial significance as described above. The interpreter must concentrate on either. In the present work the focus is on the Laxemar area where spatial significance of the shorter lineaments is honoured. Instead the extensive areas of low magnetisation, which may represent regional deformation zones, are presented explicitly as delineated areas. These areas, together with the lineaments identified, form two complementary sets of information.

4.4.2 Processing and interpretation of resistivity data

All resistivity data from the ABEM Lund Imaging System with a standard deviation higher than 1% were rejected. The gradient array protocol contains data measured with asymmetric electrode setups and standard pseudo-sections can therefore not be prepared. The data were however sorted and apparent resistivity and pseudo-depth was calculated in accordance with Figure 4-1. The gradient protocol contains a large number of electrode combinations (in pairs) similar to the uppermost two in Figure 4-1. If the influence of the remote current electrode is neglected, the average apparent resistivity of these two setups will correspond to the Schlumberger configuration at the bottom of Figure 4-1. The pseudo-depth (≈ depth of investigation) is then calculated as half the distance from the array centre to one of the current electrodes.

The resistivity data from the survey with the ABEM Lund Imaging System were entered into the inversion program RES2DINV. The data were inverted to two-dimensional models, one for each profile. A vertical/horizontal flatness filter ratio was selected in such a way that horizontal structures would be preferred. This might seem strange if sub-vertical deformation zones are the targets of the investigation. However, several tests revealed that such zones were adequately recovered with a low value (horizontal preferred) of the filter ratio. Good representation of the soil cover did however require a low filter value. So called "robust inversion" was used. This means that a model is calculated where the absolute residuals are minimized instead of the squared residuals.

The resistivity data were also entered into the program RES3DINV for three-dimensional inversion of the three survey areas. A low value for the vertical/horizontal flatness filter was chosen and robust inversion was selected (see above).

The inversion results are presented as maps where the resistivity at different depths can be observed. A few chosen vertical sections of resistivity are also presented from the inversion results in order to reflect the interpreted dip of some electrical low resistive anomaly sources.

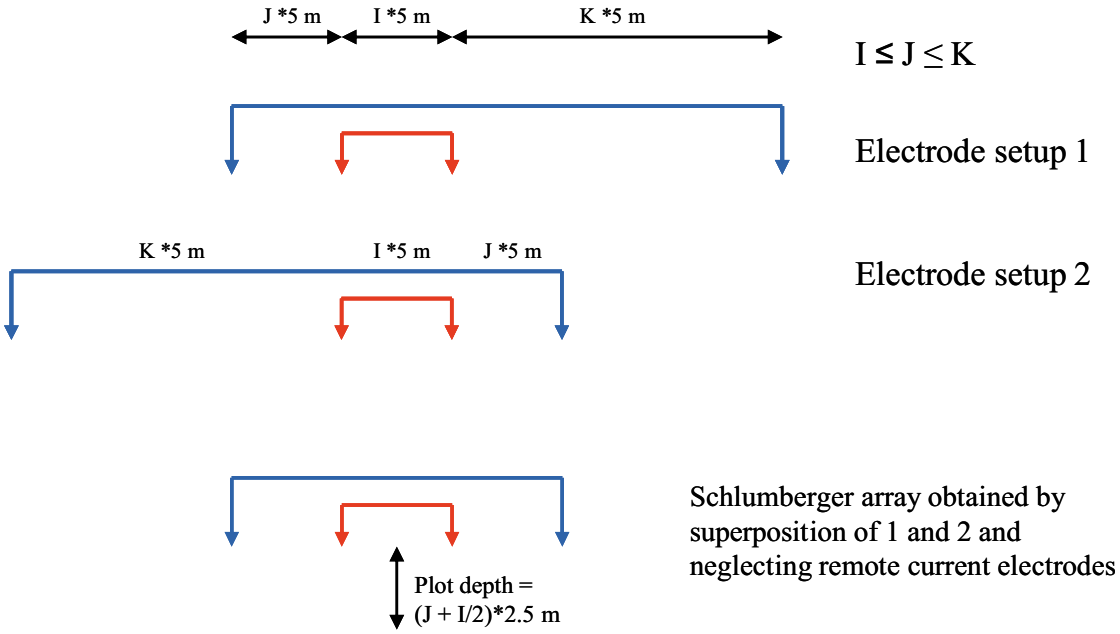

Figure 4-1. *The two top drawings show examples of electrode combinations that appear in pairs in the gradient protocol of the Lund imaging system. Current electrodes are shown in blue and potential electrodes in red. A representation of the results that can be plotted in a pseudo-section is obtained by taking the average apparent resistivity and assigning it to a combination of the two setups shown in the bottom drawing where the remote current electrodes have been neglected.*

The interpretation of resistivity data has included:

- Identification of low-resistivity anomalies in the bedrock from 2D-sections.
- Identification of lineaments in depth-slices of 3D-models.
- Joint interpretation of 2D- and 3D-results resulting in lineament maps.
- Interpretation of dips where possible.
- Interpretation of soil cover thickness.
- Interpretation of soil cover units.
- Calculation of bedrock bulk resistivity for 3D-models.

4.5 Nonconformities

In comparison to the activity plan AP PS 400-05-079 a few of the resistivity profiles had to be made shorter than originally planned. At the westernmost area, around NS001, no measurements were made close to a house. At the easternmost area a few profiles were blocked by the drill-site for KLX05.

The major power lines in the area have disturbed magnetic measurements. Data of the magnetic total field could not be used near the power lines. The affected areas are easily recognised in the maps of the magnetic total field as blanked areas. A few small areas close to houses and at drill sites could not be measured.

5 Results

The results are stored in the primary data bases (SICADA and/or GIS). The data is traceable in SICADA and GIS by the Activity Plan number (AP PS 400-05-079).

5.1 The magnetic total field

A map showing a mosaic of the presented ground geophysical survey together with the magnetic survey from spring 2005 /8/ can be seen in Figure 5-1. The magnetic total field from the helicopter-borne survey /9, 10/ is shown in the background. The data sets have been reduced to the pole; however they are displayed with different colour scales.

The map of the magnetic total is shown as a grey-scale image in Figure 5-2 and as a shaded relief image, enhancing the appearance of narrow features, in Figure 5-3.

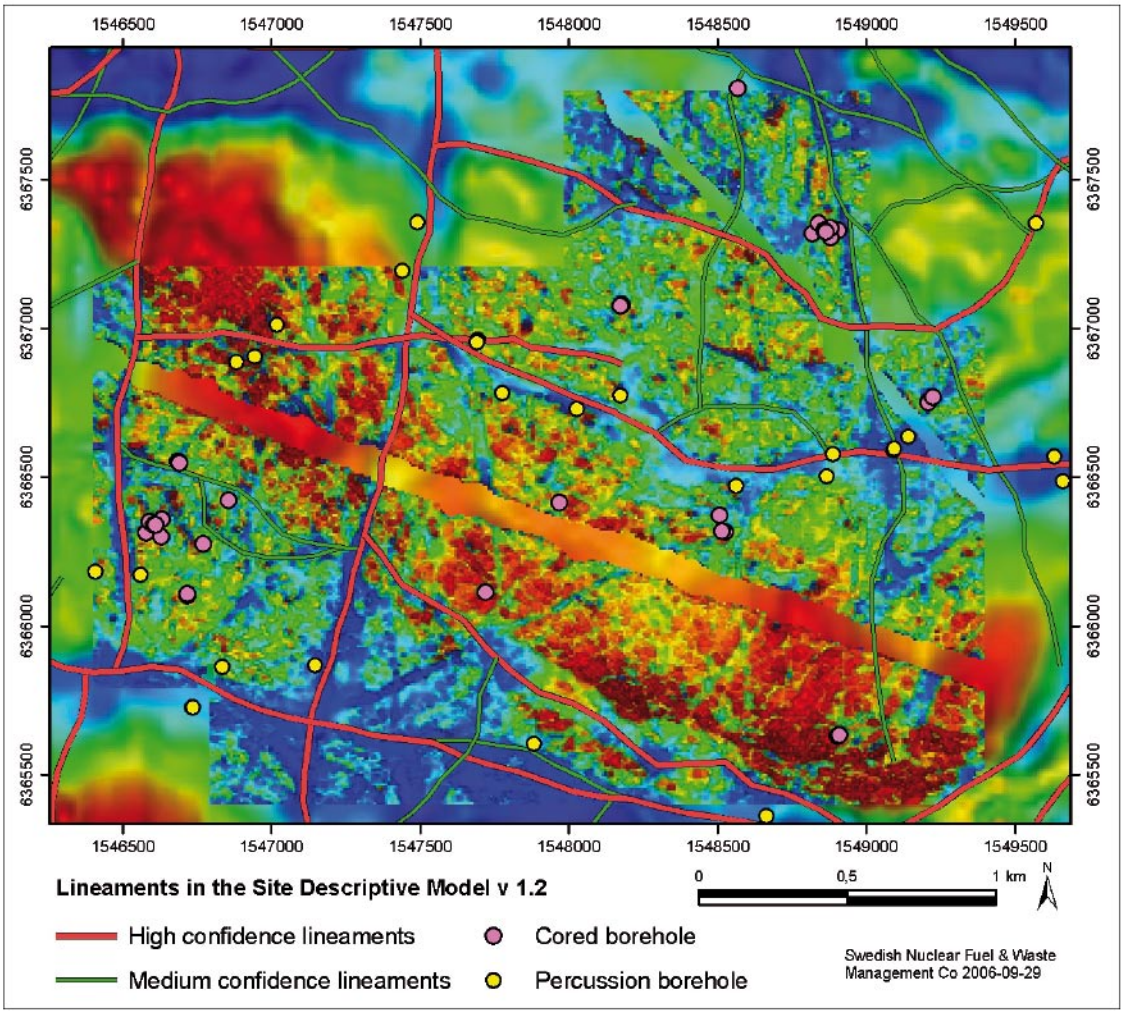

Figure 5-1. *The magnetic total field from the detailed ground geophysical surveys of 2005 displayed on the magnetic total field from the helicopter-borne survey of 2002. The data sets are reduced to the pole. Different colour scales have been applied.*

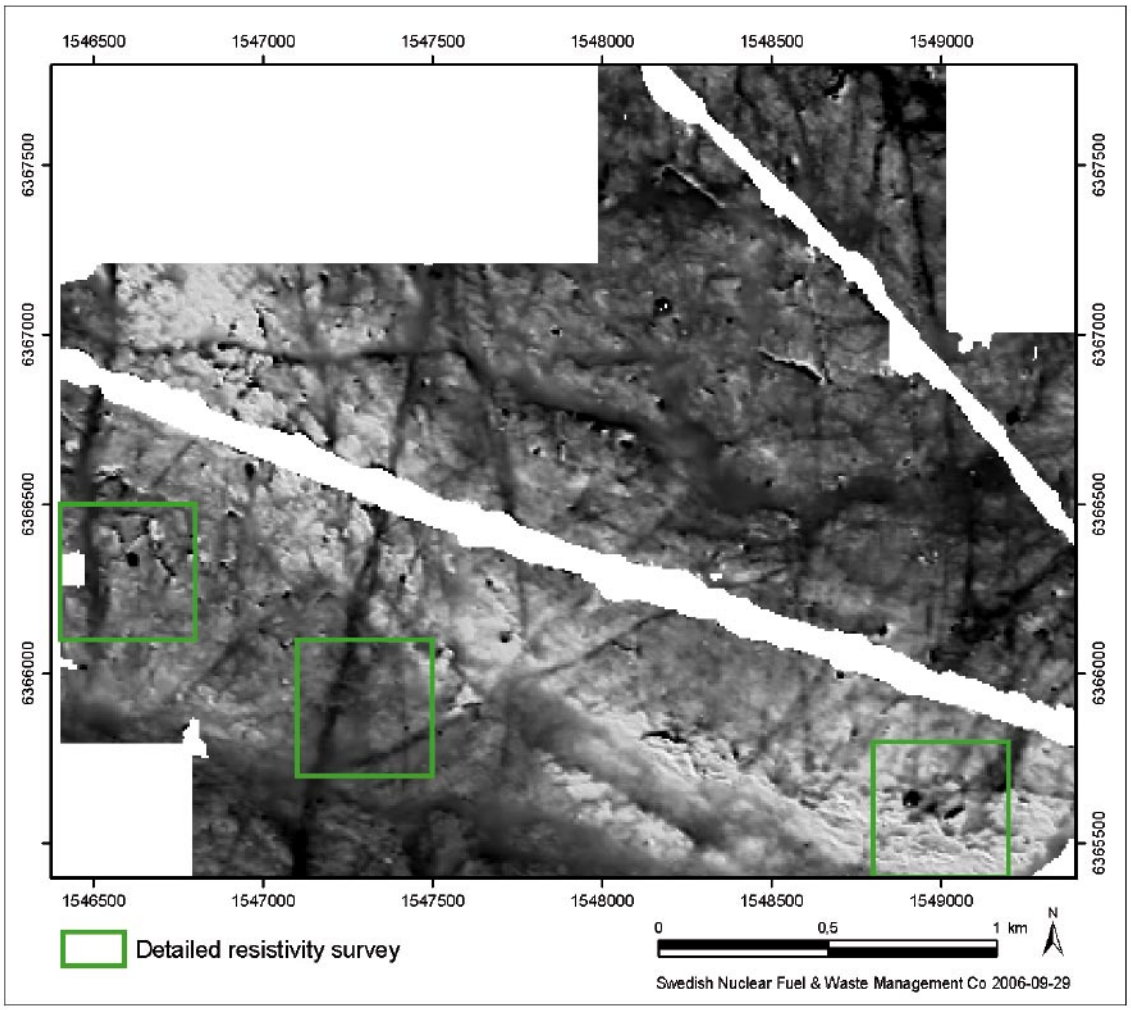

Figure 5-2. *Magnetic total field from detailed ground surveys shown as a greyscale image. Positive anomalies are shown as bright and negative anomalies as dark shades. The three areas covered by detailed resistivity measurements are shown as green quadrates.*

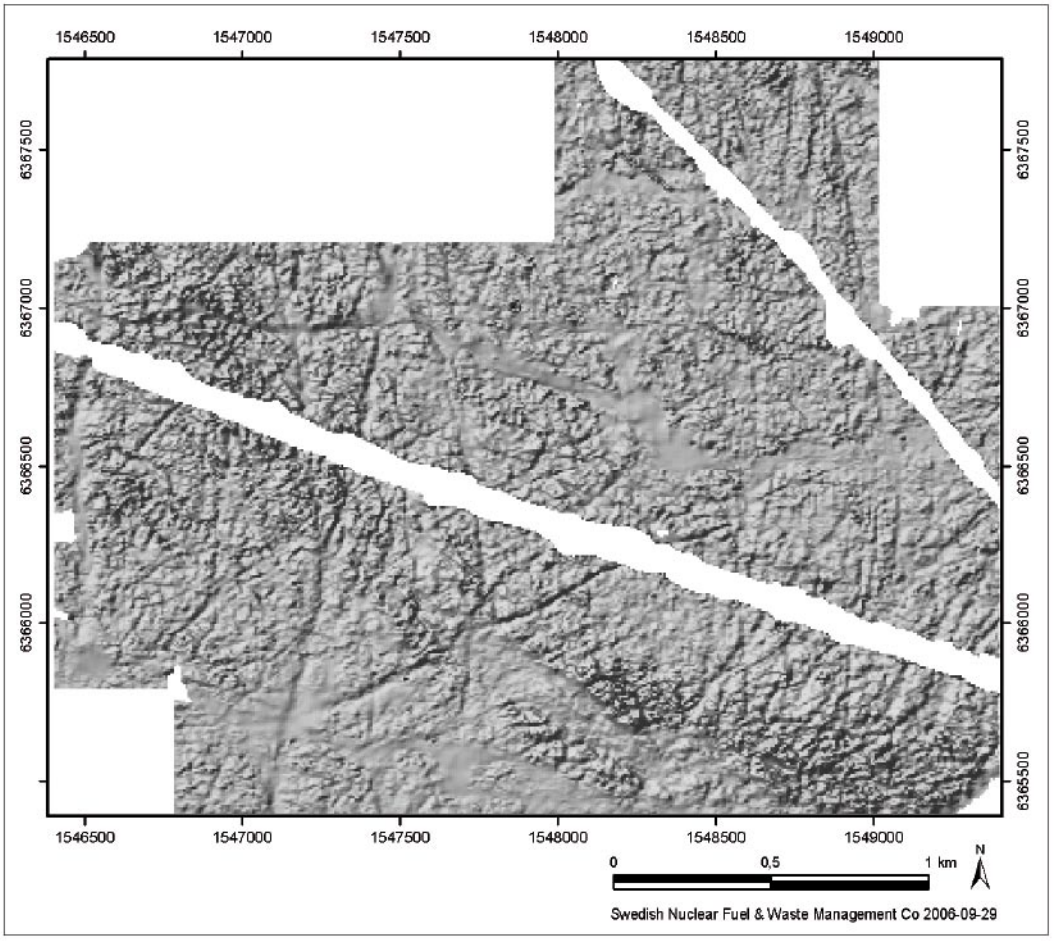

Figure 5-3. *Magnetic total field from detailed ground surveys shown as shaded relief image. Illumination is from north-west.*

5.2 The electric resistivity

The apparent resistivity from different depth slices (see Section 4.4.2) are presented in Figures 5-4, 5-5 and 5-6. The location of the three detailed resistivity survey areas can be seen in Figure 1-1 and in Figure 5-2.

Examples of apparent resistivity pseudo-sections are shown in Figures 5-7, 5-8 and 5-9. One representative section for each area is shown. They are plotted with the same colour scale as the depth-slice maps above.

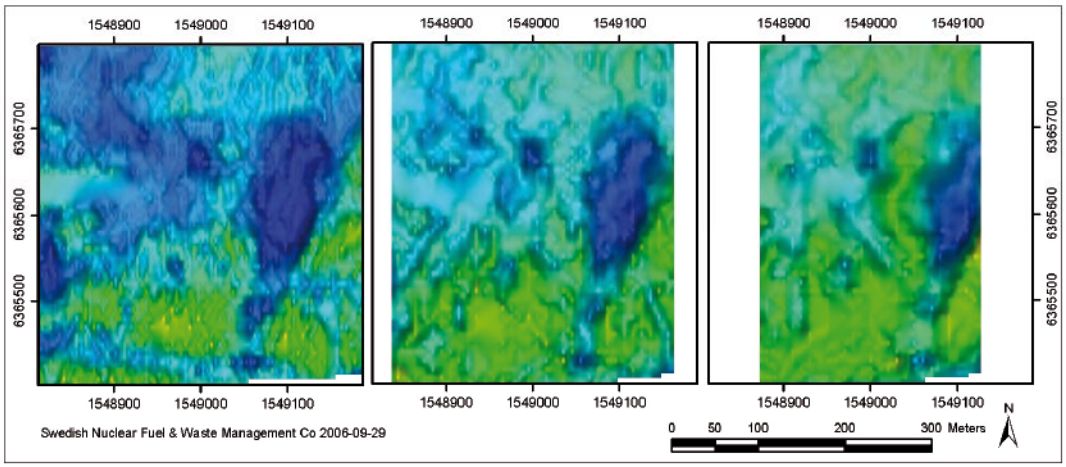

Figure 5-4. *Apparent resistivity depth slices from the eastern survey area (around NS046). The pseudo-depths are, from left to right, 6.25 m, 17.5 m and 35 m respectively. Colour-scale according to Figure 5-10.*

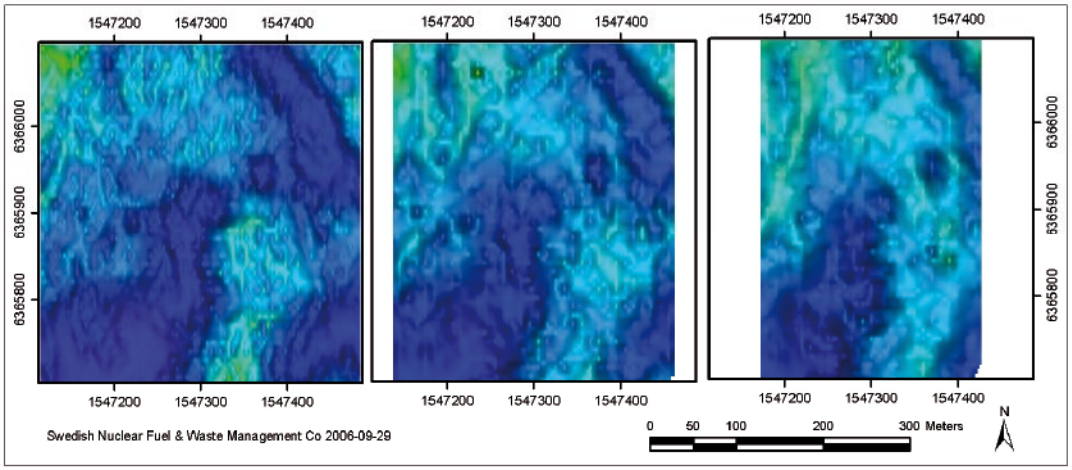

Figure 5-5. *Apparent resistivity depth slices from the central survey area (around NS059). The pseudo-depths are, from left to right, 6.25 m, 17.5 m and 35 m respectively. Colour-scale according to Figure 5-10.*

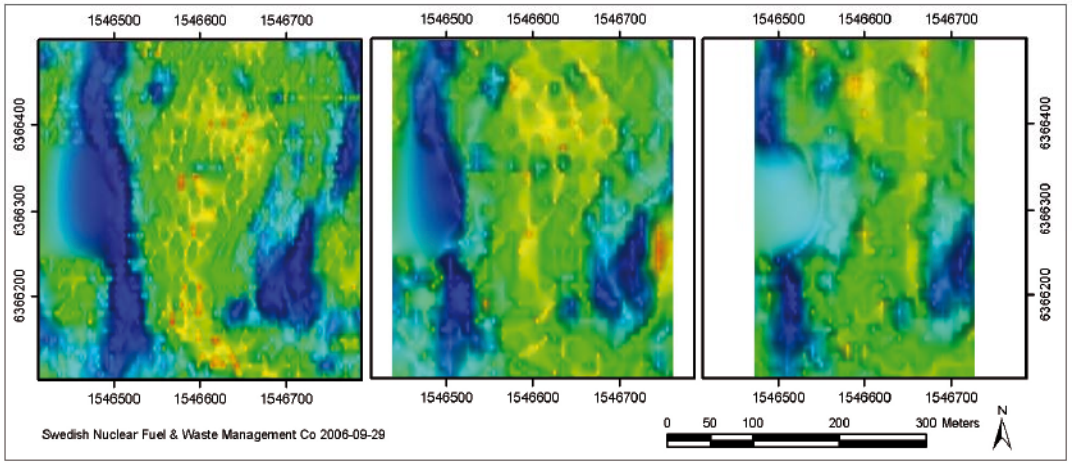

Figure 5-6. *Apparent resistivity depth slices from the western survey area (around NS001). The pseudo-depths are, from left to right, 6.25 m, 17.5 m and 35 m respectively. Colour-scale according to Figure 5-10.*

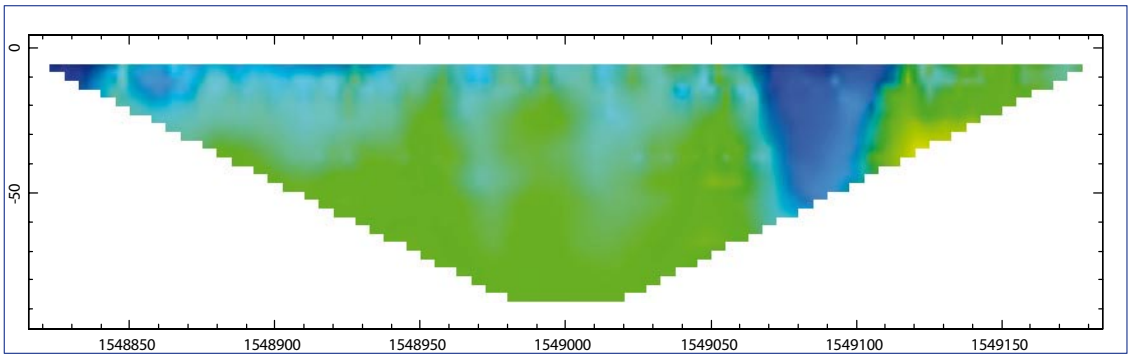

Figure 5-7. *Apparent resistivity pseudo-section, 6365500N, from the eastern survey area (around NS046). Colour-scale according to Figure 5-10.*

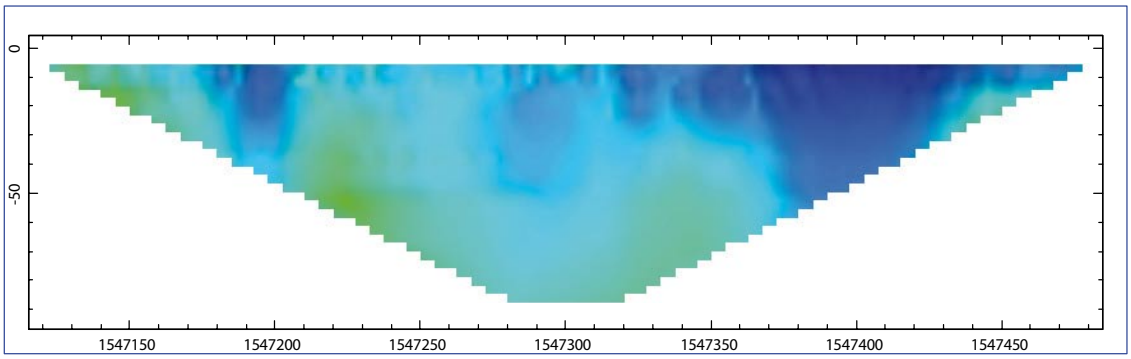

Figure 5-8. *Apparent resistivity pseudo-section, 6366050N, from the central survey area (around NS059). Colour-scale according to Figure 5-10.*

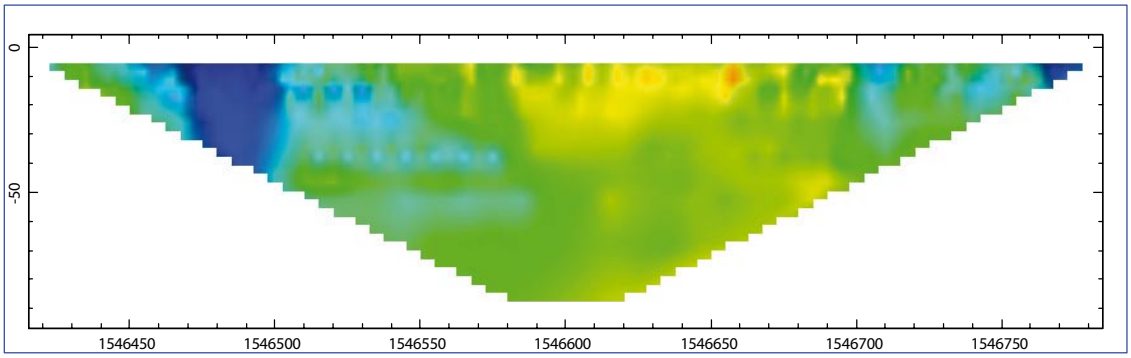

Figure 5-9. *Apparent resistivity pseudo-section, 6366390N, from the western survey area (around NS001). Colour-scale according to Figure 5-10.*

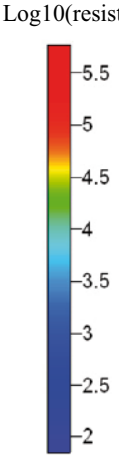

Figure 5-10. *Colour scale used for all resistivity plots in this section and below.*

5.3 Lineaments identified in magnetic total field data

Lineaments have been identified in data of the magnetic total field. Furthermore, extensive areas with low magnetisation have been delineated. During the procedure of lineament identification also lineaments earlier presented /8/ were re-evaluated. The reason is that the new measurements have increased the area covered by dense measurements of the magnetic total field where the view of a large area favours identification of subtle anomaly patterns.

In the magnetic total field data some linear anomalies with strange characteristics occurred. In the earlier version of magnetic lineaments presented, such anomalies were also included as lineaments though their characteristics strongly indicated the source to be related to roads or fences. In the current version of lineaments they are however excluded.

Lineaments identified in the magnetic total field from the ground magnetic measurements are shown in Figure 5-11. More than 2,000 lineaments were identified.

The parameter “Uncertainty” has been classified and its variation is displayed in Figure 5-12 together with extensive areas of low magnetization.

In Figure 5-13 the current version of the structural part of the Site Descriptive Model version 1.2 /19/ is shown together with the lineaments. It is obvious that EW007 and NW042A are not well described by the lineaments in the current work, as opposed to the results from joint interpretations of longer lineaments /13/. The reason is the extensive areas of low magnetisation coinciding with the two features; the problem is discussed in Section 4.4.1 above.

Some of the features in the Site Descriptive model version 1.2 have become more resolved by the current work. As an example at least the northern part of the feature NE138A appears doubtful and may not exist. The southernmost part of NS046A is also debatable and the existence of NW932C is not supported by the current work.

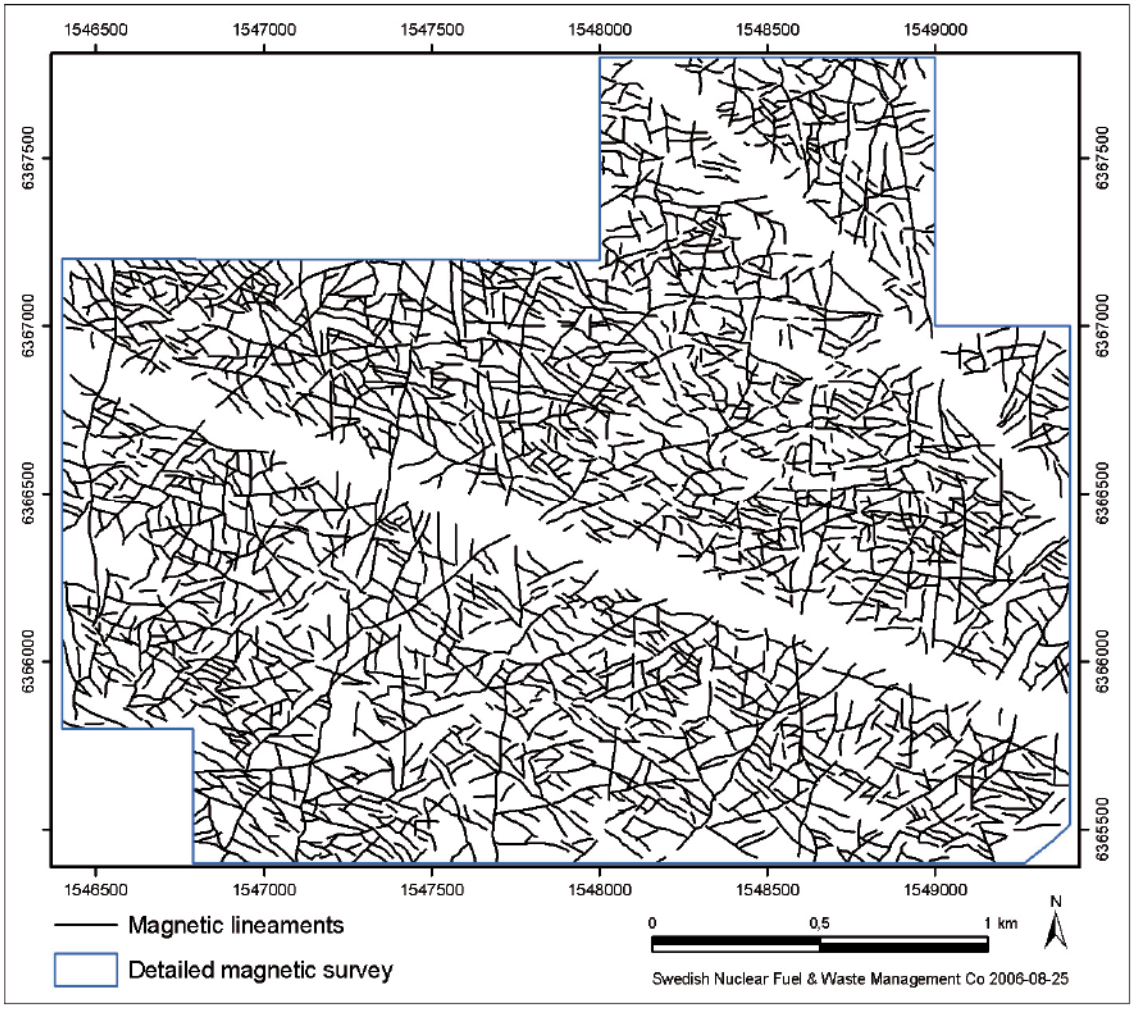

Figure 5-11. *The lineaments identified in magnetic total field data.*

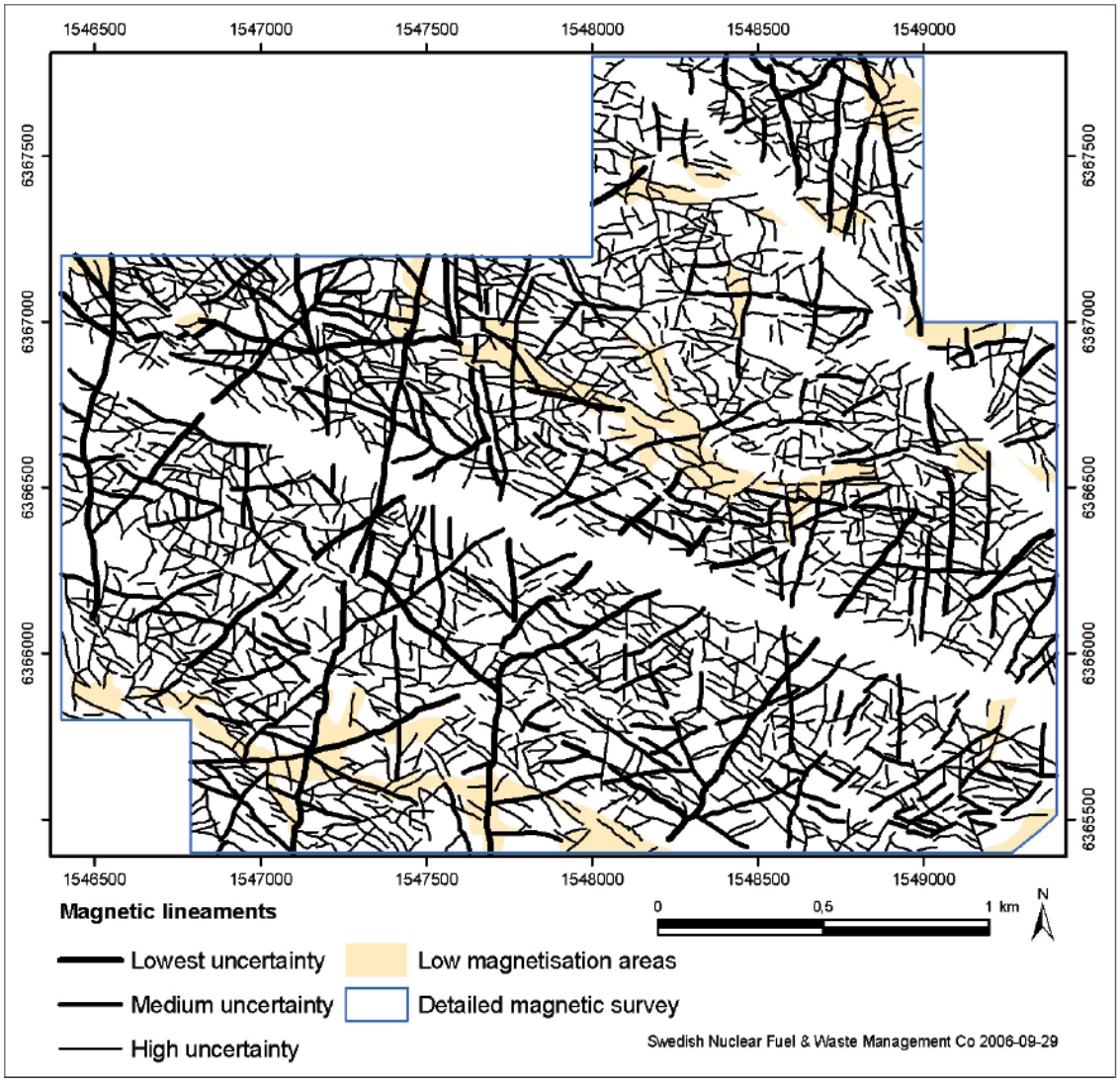

Figure 5-12. *The lineaments identified in magnetic total field data with the parameter Uncertainty displayed.*

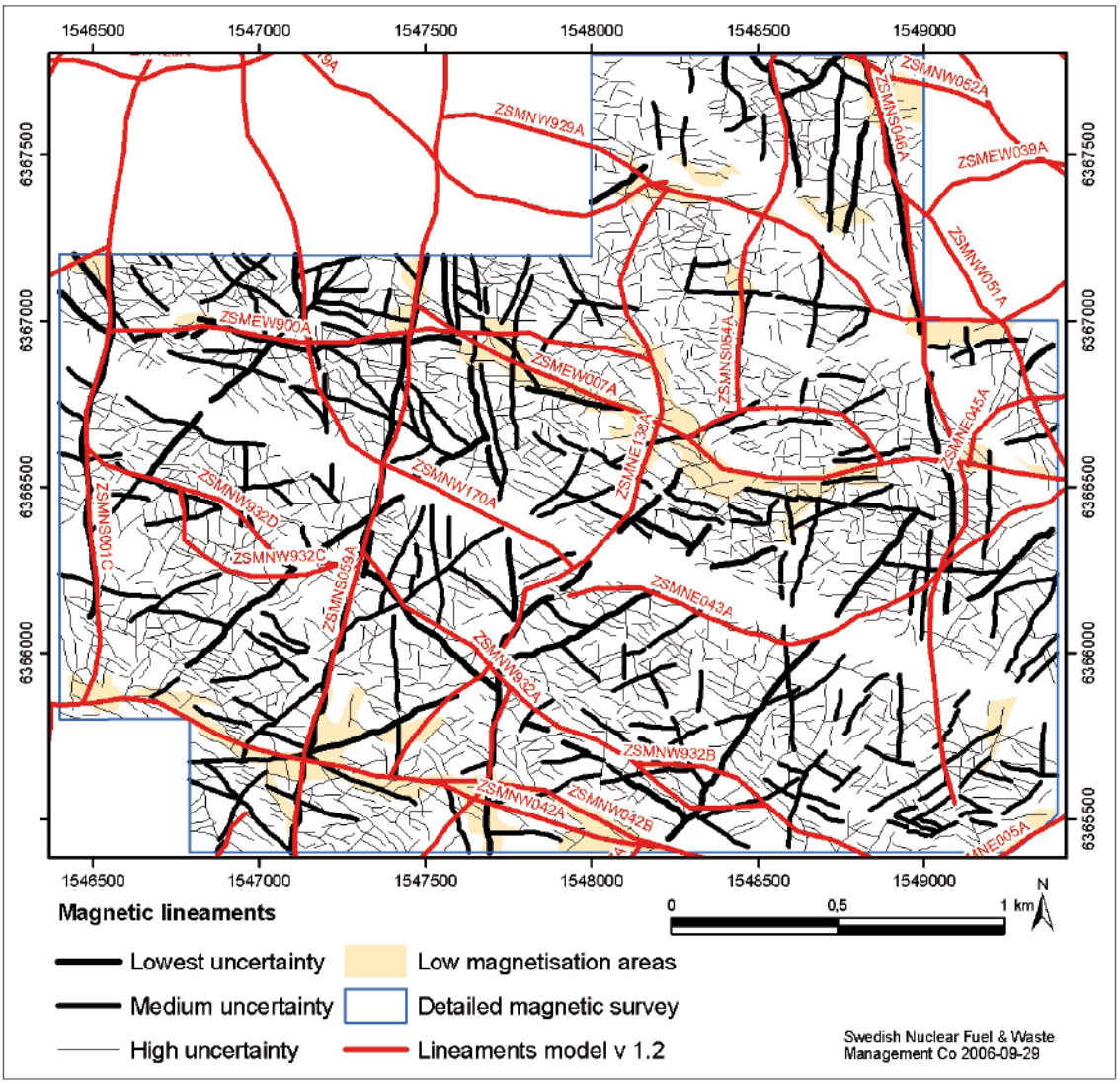

Figure 5-13. *The lineaments identified in magnetic total field data (in black) displayed together with the structural part of Laxemar site model 1.2 (in red) /19/.*

5.4 Numerical modelling of magnetic data

5.4.1 Voxel based inversion of magnetic data

The magnetic data were inverted to voxel models in different scales of resolution. It is not practically possible to obtain reliable results for both local detail and large scale features at the same time. A regional model was first obtained for the entire Laxemar area. Two models of the south-western and south-eastern part of Laxemar (Figure 5-14) respectively were thereafter produced in an intermediate scale of resolution. Finally, two detailed models were found for the south-eastern part of the Laxemar area (Figure 5-14).

A mosaic of data of the magnetic total field as measured on ground and from helicopter was produced, where the latter were levelled by matching the mean value to the ground results. Both data sets were first reduced to the pole. It is not formally correct to produce a mosaic in this manner since the data have been acquired at different datum levels. The helicopterborne data were however mainly introduced in order to avoid inversion artefacts due to edge effects.

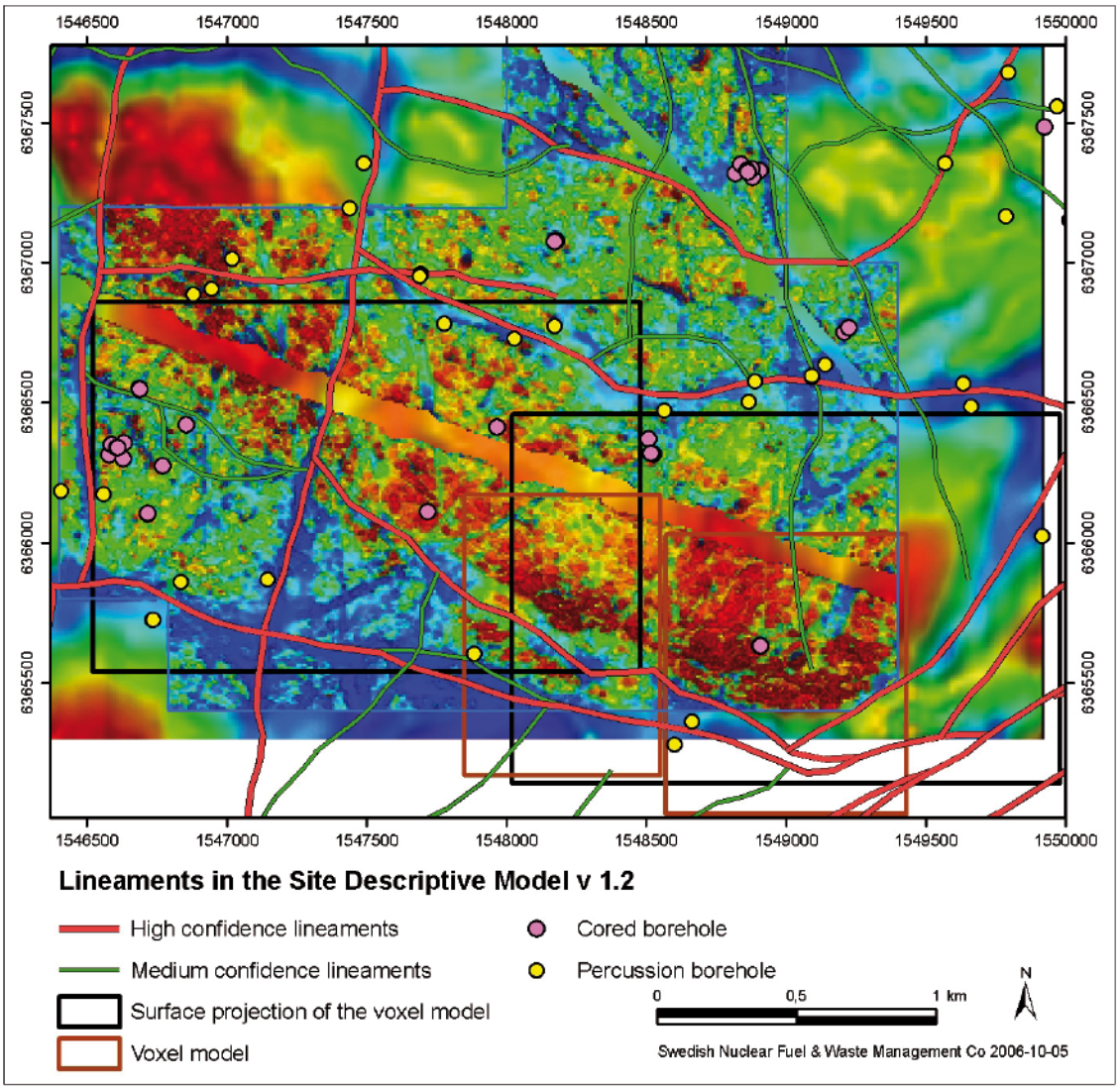

Figure 5-14. *Ground and helicopter-borne magnetic data from Laxemar. The two black rectangles show the surface projection of the voxel models in Figures 5-16 to 5-19. The western brown rectangle corresponds to the voxel model in Figure 5-20 and the eastern brown rectangle to the model in Figure 5-21.*

The data were also upward continued in later processing steps and the effect of datum level differences was thereby reduced.

Magnetic measurements are very much affected by local anomalies due to near-surface rock of high magnetization. Pseudo-gravity inversion was therefore performed to produce a data set that will provide more information about regional features. This data set was then upward continued to 600 m and the residual was inverted to a voxel model. The use of a residual will provide data with wave-lengths corresponding to sources at depths up to a few hundred metres.

An iso-surface corresponding to a moderately high magnetic susceptibility can bee seen in Figure 5-15. The volume enclosed by the iso-surface roughly corresponds to diorite/gabbro and the more magnetic type of Ävrö-granite near the surface. The northern border of the main volume dips to the north and intersects KLX10 at roughly 170 m borehole depth and KLX08 at approximately 490 m borehole depth. The southern border of the main magnetized volume dips sub-vertically and intersects KLX03 with a small angle.

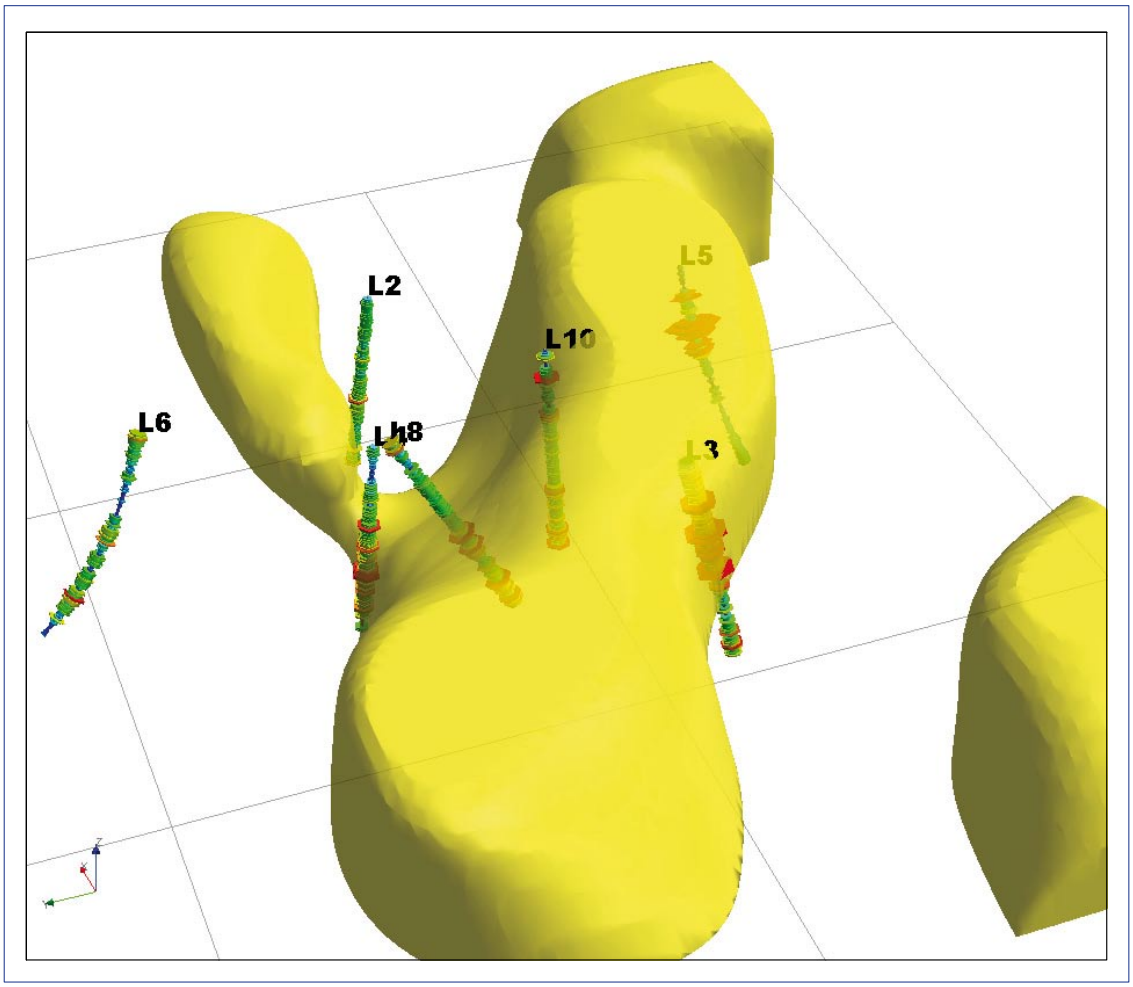

Figure 5-15. *Iso-surfaces corresponding to a voxel-based inversion model of pseudo-gravity integrated magnetic data. The closed volumes correspond to moderate/high magnetization in the model. Cored boreholes are shown with colour and diameter indicating measured magnetic susceptibility (red = high) in borehole logging (L2 = KLX02 etc). The model is viewed from WNW.*

The ground/helicopterborne magnetic data were upward continued to 40 m and subsets slightly larger than the black rectangles in Figure 5-14 were extracted. Voxel inversions were performed and the models were cropped to fit the black rectangles in Figure 5-14. A three-dimensional view of iso-surfaces enclosing volumes with magnetic susceptibilities above 0.06 SI in both models can be seen in Figure 5-16. The surface projection of these volumes corresponds well to occurrences of diorite/gabbro at a border-zone between the Ävrö-granite and quartz monzodiorite. The magnetic volumes dip steeply towards north in the area between KLX03 and KLX05. Sub-vertical dips are seen further east. The models extend to 480 m depth, although they are less reliable in the deeper parts.

Iso-surfaces enclosing volumes with magnetic susceptibility above 0.03 SI can be seen in Figure 5-17. Such volumes are abundant in areas corresponding to Ävrö-granite at the surface. However, in those areas mapped as quartz monzodiorite at the surface, magnetic volumes are only found in the west, between NS001 and NS059. A fairly large volume around NS059 is low-magnetic.

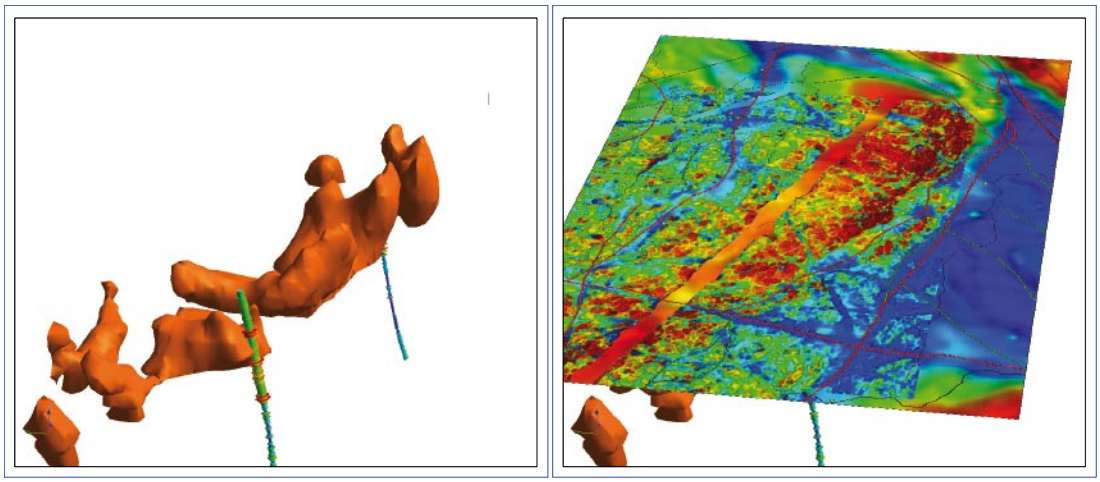

Figure 5-16. *Iso-surfaces corresponding to voxel-based inversion models of the areas marked with black rectangles in Figure 5-14. The closed volumes correspond to magnetic susceptibility above 0.06 SI. KLX03 in the front and KLX05 in the back are shown with colour and diameter indicating measured magnetic susceptibility (red=high) in borehole logging. The upper part of KLX05 is inside a closed iso-surface. The model is viewed from WSW. The magnetic map is overlain in the right image for geographic reference.*

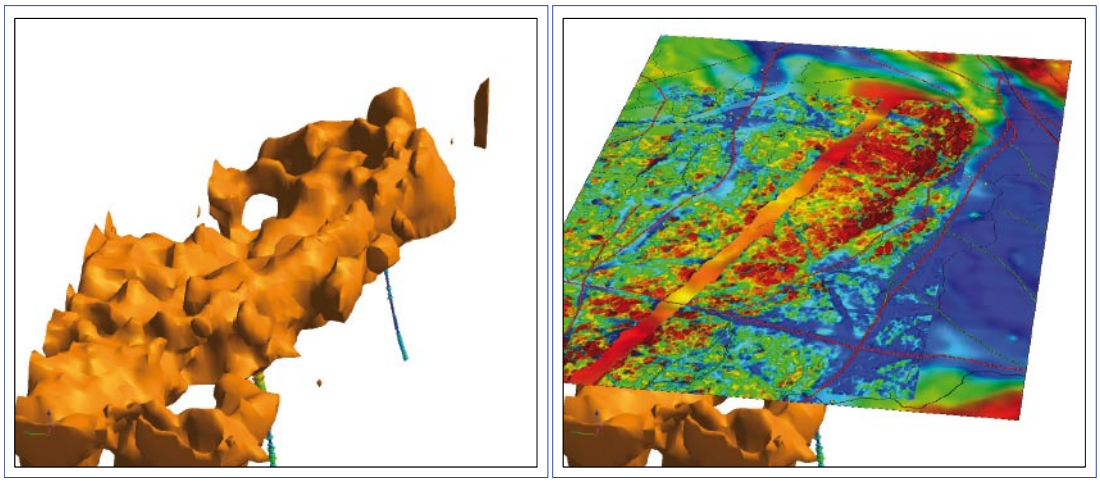

Figure 5-17. *Iso-surfaces corresponding to voxel-based inversion models of the areas marked with black rectangles in Figure 5-14. The closed volumes correspond to magnetic susceptibility above 0.03 SI. KLX03 in the front and KLX05 in the back are shown with colour and diameter indicating measured magnetic susceptibility (red=high) in borehole logging. The model is viewed from WSW. The magnetic map is overlain in the right image for geographic reference.*

Three-dimensional views with the iso-surfaces described above underneath semi-transparent versions of the bedrock geology map can be found in Figures 5-18 and 5-19. The correspondence between occurrences of diorite/gabbro (green) at the surface and strongly magnetic volumes can be seen in Figure 5-18, whereas the abundance of intermediate magnetic rocks on areas of Ävrö-granite in the southern part of Laxemar can be seen in Figure 5-19.

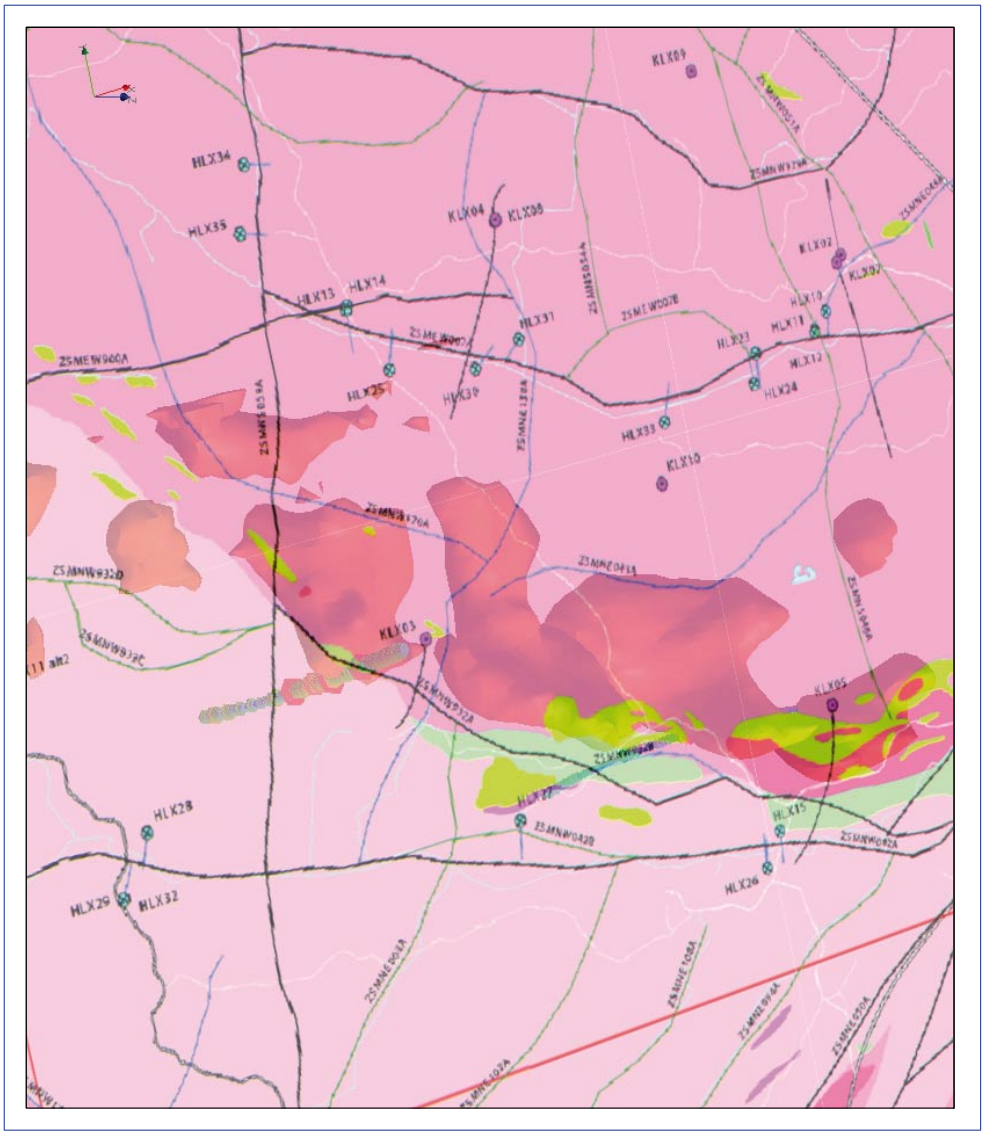

Figure 5-18. *Iso-surfaces enclosing magnetic volumes (see Figure 5-16) underneath a semi-transparent version of the bedrock geological map. The pink colour to the left corresponds to Ävrö-granite whereas the brighter pink to the right corresponds to quartz monzodiorite. Yellowish green indicates occurrences of diorite/gabbro.*

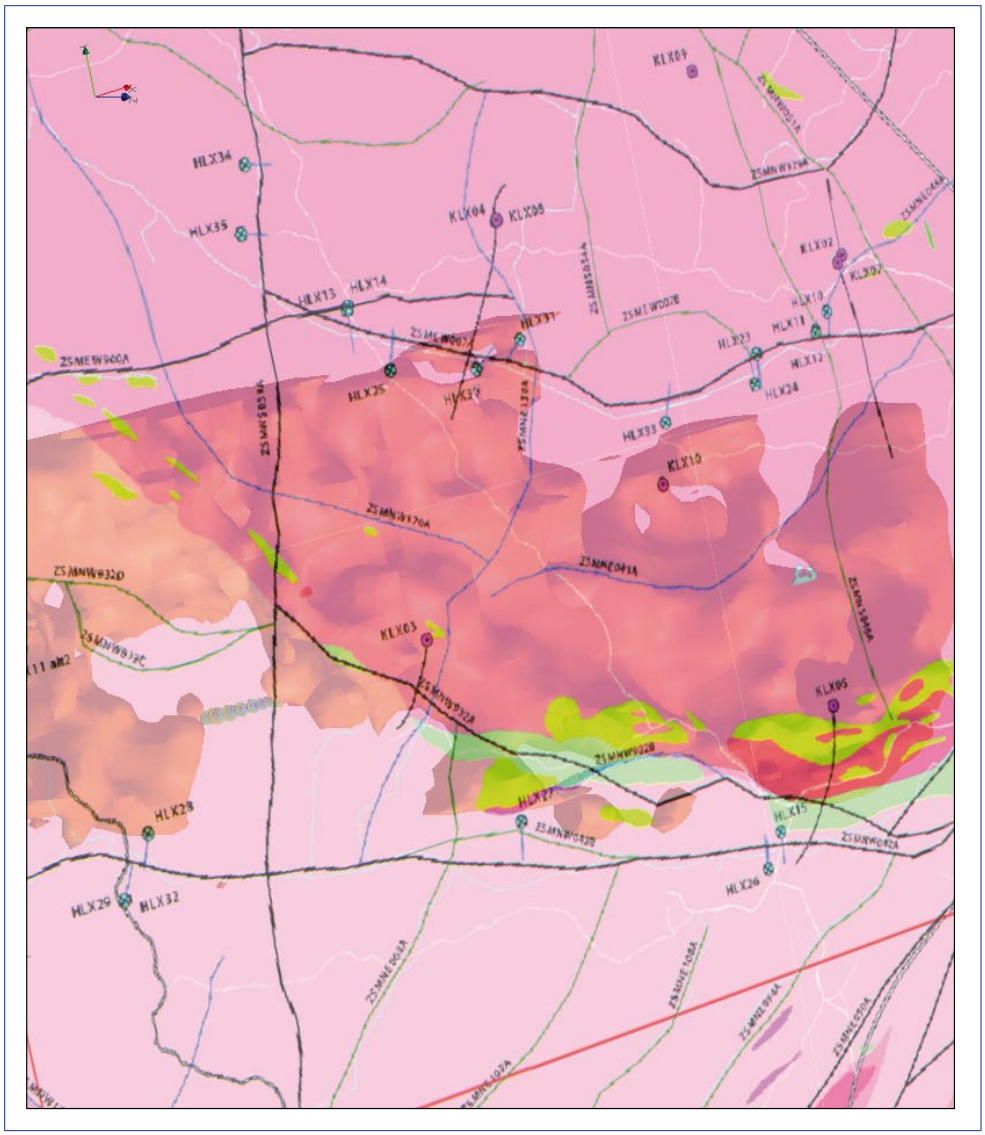

Figure 5-19. *Iso-surfaces enclosing intermediately magnetic volumes (see Figure 5-17) underneath a semi-transparent version of the bedrock geological map. The pink colour to the left corresponds to Ävrö-granite whereas the brighter pink to the right corresponds to quartz monzodiorite. Yellowish green indicates occurrences of diorite/gabbro.*

Detailed voxel inversion models have been created for the areas marked with magenta rectangles in Figure 5-14. The magnetic data were first upward continued 15 m. A steep dip to the north for the magnetic volumes between KLX03 and KLX05 can be seen in Figure 5-20 (the western area). A small magnetic "satellite" enclosed by quartz monzodiorite further south can be seen to have very limited down-dip extent. The rocks in the eastern area in Figure 5-21 are more magnetic. The indicated dip is steep towards north in this area as well. The indicated dip fits well with logged magnetic susceptibility in KLX05. The model is unfortunately biased towards low susceptibility close to KLX05 due to negative magnetic anomalies due to man-made objects at the drill-site.

Several attempts were made to perform voxel inversions of magnetic data around the negative anomalies that are associated with deformation zones. However, no results that seemed geologically meaningful came out of this work. It is possible that inversion routines constrained by smoothness not are appropriate for such low-magnetic features but it can also not be ruled out that the geometry towards depth of such features is poorly constrained by the magnetic data.

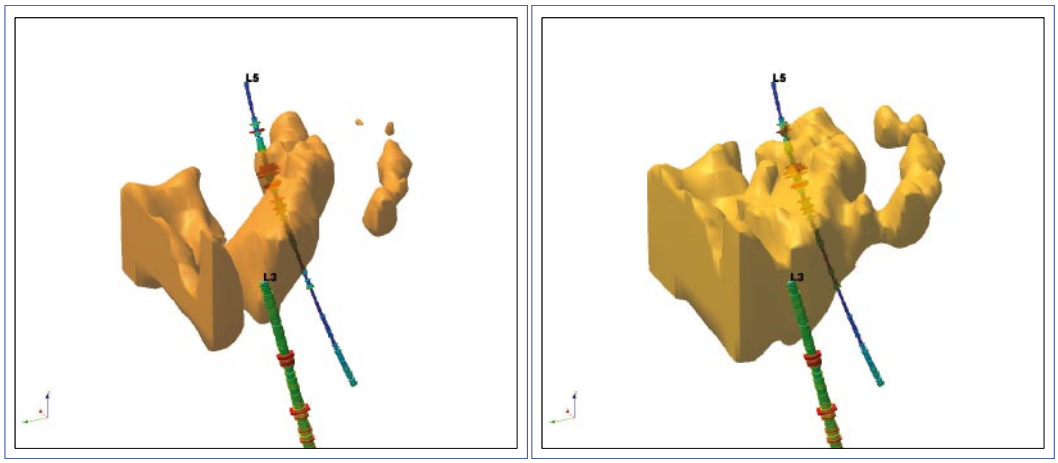

Figure 5-20. *Iso-surfaces corresponding to a voxel-based inversion model of the western area marked with a magenta rectangle in Figure 5-14. The closed volumes correspond to magnetic susceptibility above 0.05 SI (left) and 0.035 SI (right). KLX03 is in front of the model and KLX05 behind. The model is viewed from WNW.*

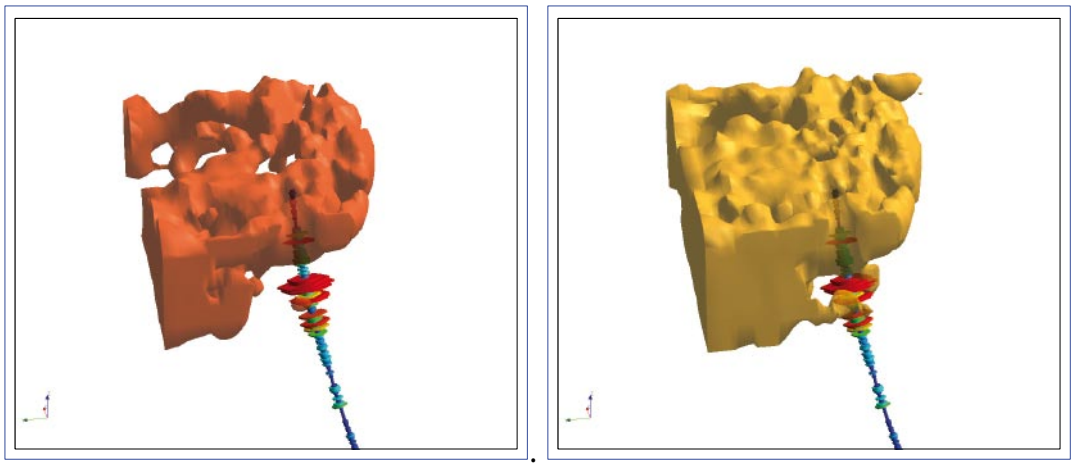

Figure 5-21. *Iso-surfaces corresponding to a voxel-based inversion model of the eastern area marked with a magenta rectangle in Figure 5-14. The closed volumes correspond to magnetic susceptibility above 0.05 SI (left) and 0.035 SI (right). The upper part of KLX05 is inside the model. The model is viewed from WNW. The volume around KLX05 is biased towards low susceptibility values due to man-made magnetic anomalies.*

5.4.2 Forward modelling of magnetic data

Forward modelling of the four structures EW007, NS001, NS059 and a north-east striking lineament have yielded indications of the geometric complexity and dip. The modelling was carried out on five profiles over EW007, one over NS001, two over NS059 and two over the north-east striking lineament, see Figure 5-22 for modelled profile locations.

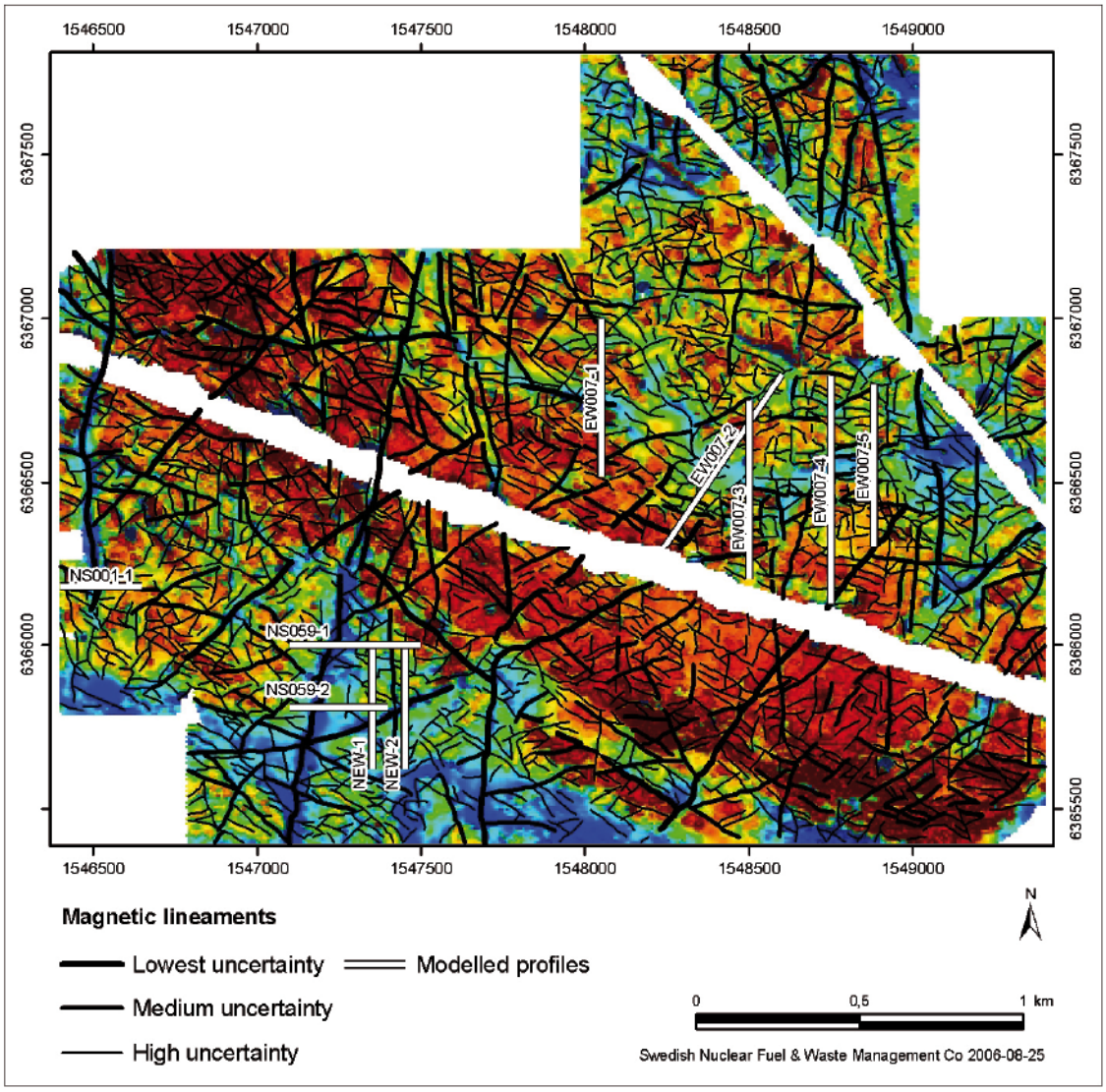

Figure 5-22. *Location of profiles with forward modelling of magnetic total field data. EW007 is covered by five profiles (EW007-1 to EW007-5), NS059 by two profiles (NS059-1 and NS059-2), NS001 by one profile (NS001-1) and a north-east striking lineament by two profiles (NEW-1 and NEW-2). The results are displayed in Figures 5-23 to 5-32.*

The results are almost self-explaining and can be viewed in Figures 5-23 to 5-32. Forward modelling of magnetic data was also carried out in an earlier activity of some lineaments in the area /8/.

North-east-striking lineament

The modelling results in an almost vertical dip of the low magnetic source body (Figures 5-23 and 5-24).

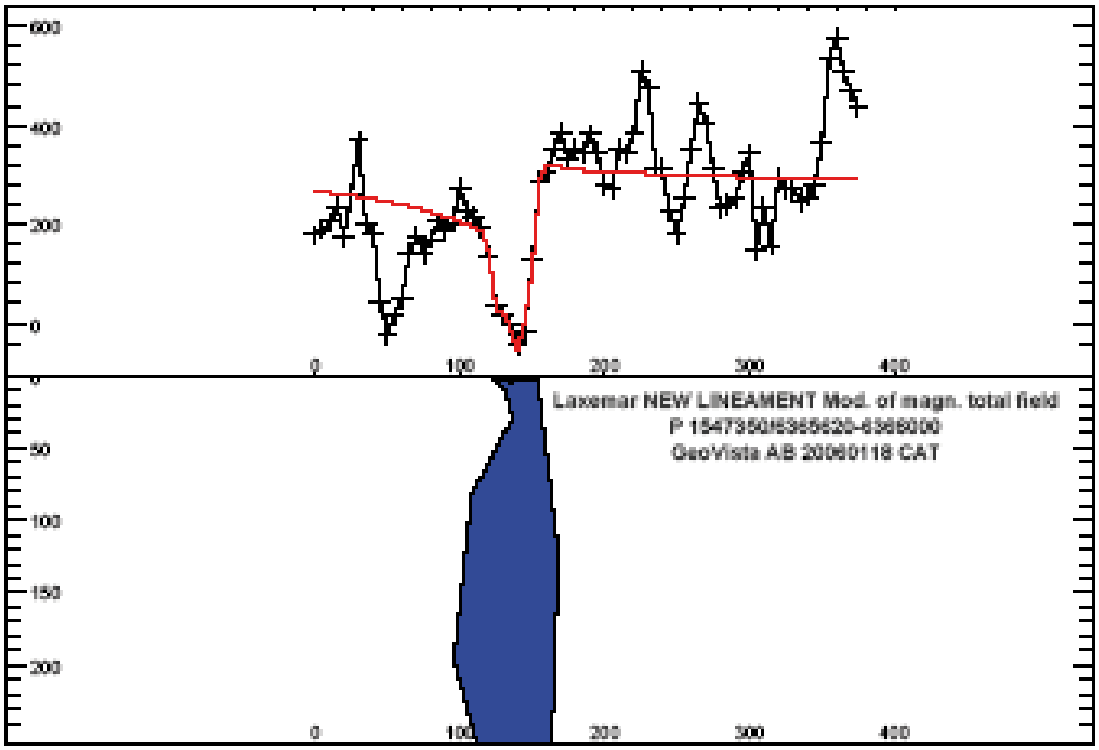

Figure 5-23. *Forward modelling of magnetic total field data over north-east striking lineament (profile NEW-1). North is towards right in the figure.*

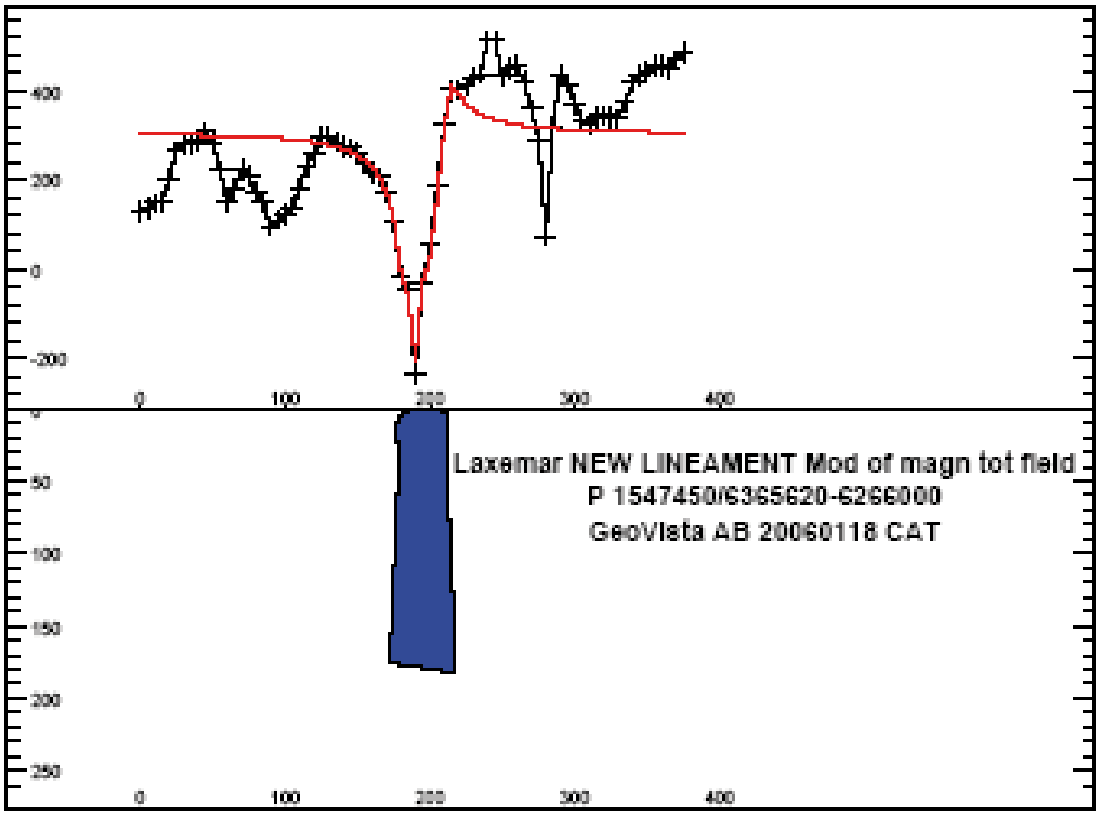

Figure 5-24. *Forward modelling of magnetic total field over north-east striking lineament (profile NEW-2). North is towards right in the figure.*

EW007

EW007 was also partly modelled previously /8/. Five modelled profiles (Figures 5-25 to 5-29) are presented here. The dip varies between slightly towards north and slightly towards south. The geometric complexity of EW007 is well displayed in the modelling results.

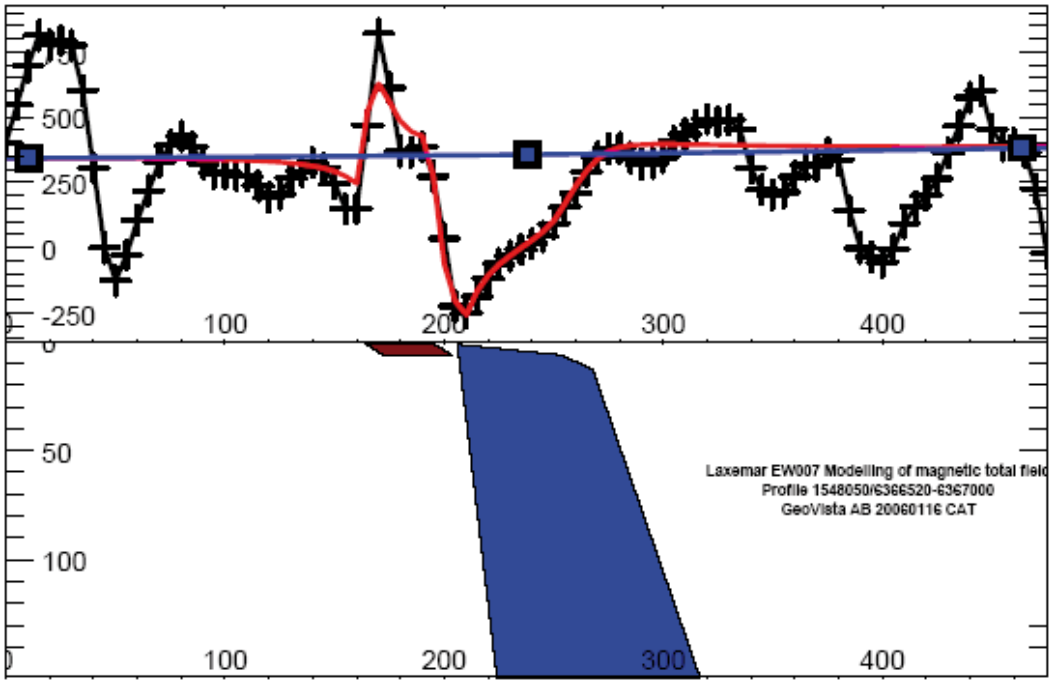

Figure 5-25. *Forward modelling of magnetic total field data over EW007 (profile EW007-1). The blue source body marks the EW007. North is towards right in the figure. Blue bodies have low relative magnetic susceptibility.*

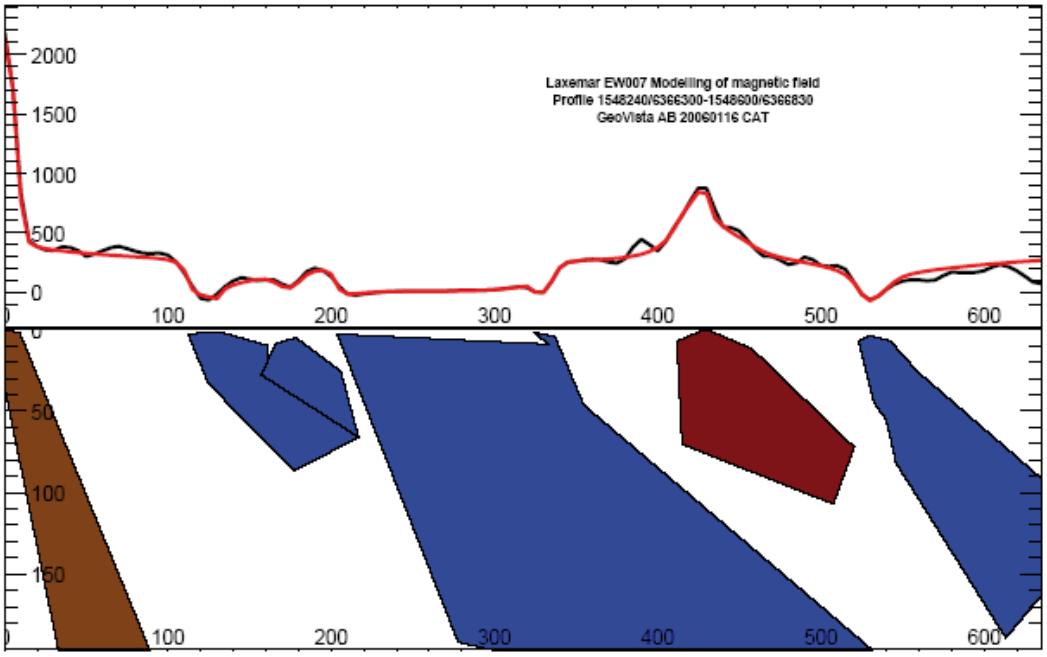

Figure 5-26. *Forward modelling of magnetic total field data over EW007 (profile EW007-2). Here EW007 is complex – all three blue source bodies at left represent it. North-east is towards right in the figure. Blue bodies have low relative magnetic susceptibility.*

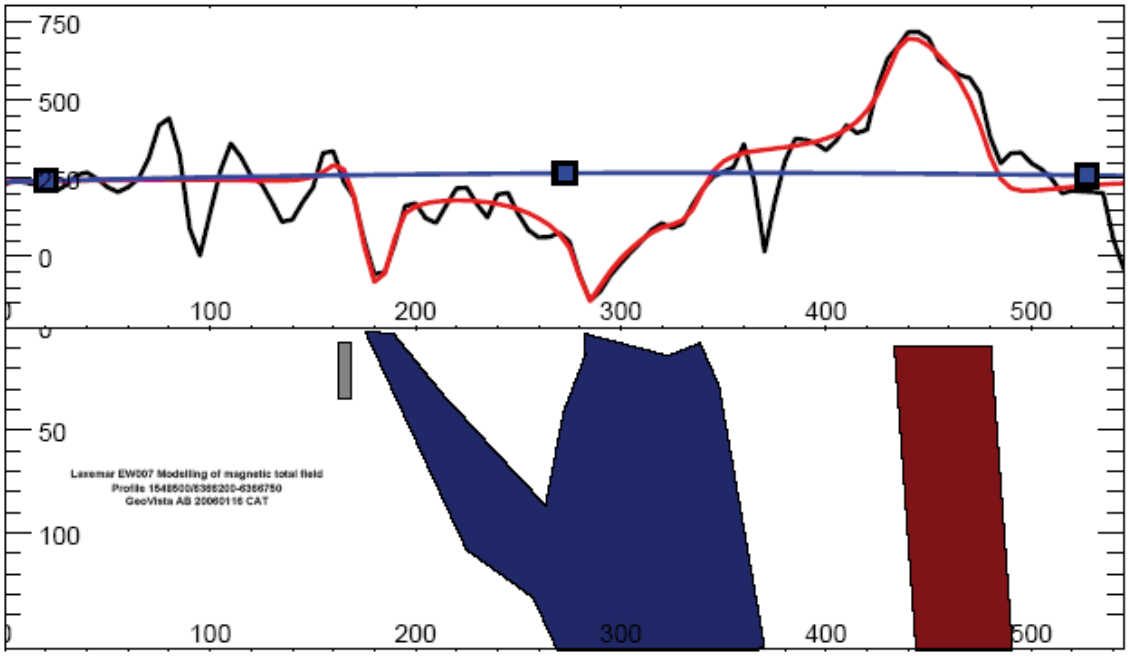

Figure 5-27. *Forward modelling of magnetic total field data over EW007 (profile EW007-3). The blue source body at centre of the figure represents EW007. North is towards right in the figure. Blue bodies have low relative magnetic susceptibility.*

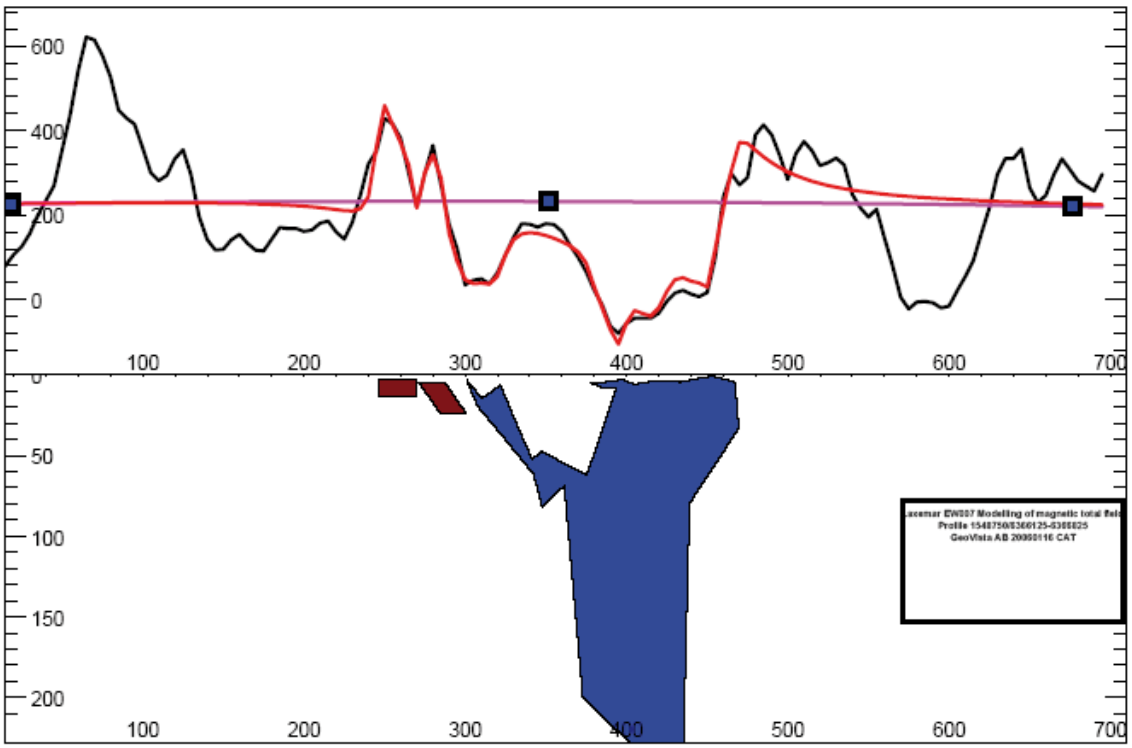

Figure 5-28. *Forward modelling of magnetic total field data over EW007 (profile EW007-4). The blue source body at centre of the figure represents EW007. North is towards right in the figure. Blue bodies have low relative magnetic susceptibility.*

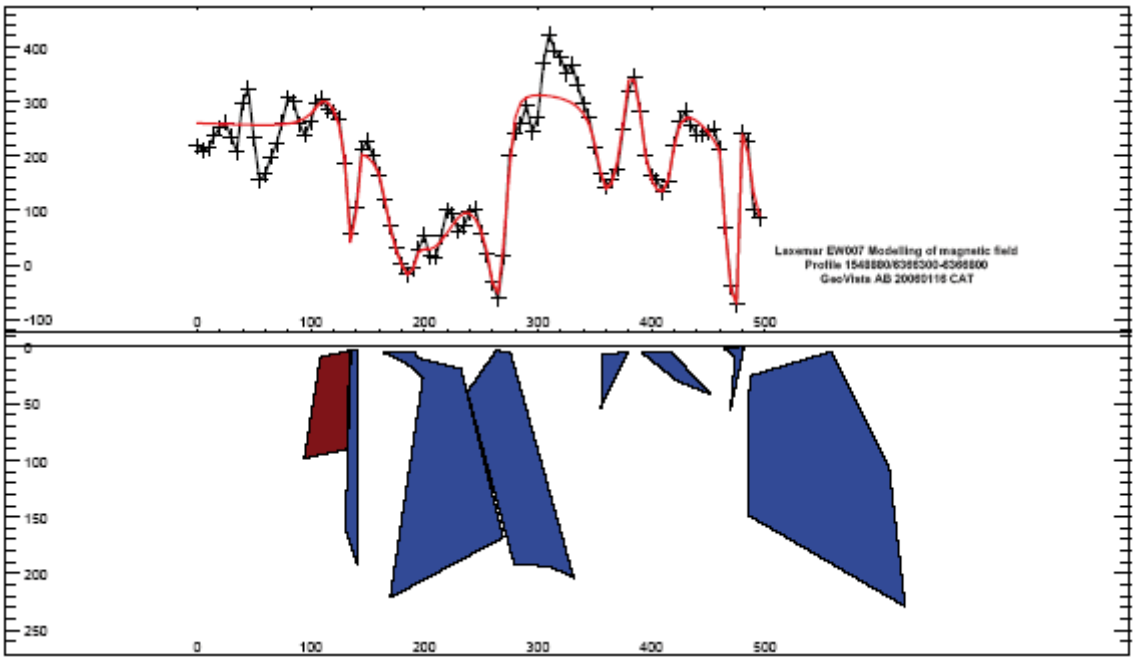

Figure 5-29. *Forward modelling of magnetic total field data over EW007 (profile EW007-5). The three blue bodies at the left of the figure represent EW007. The large blue body at right is only modelled for the purpose of adjusting the background level. North is towards right in the figure. Blue bodies have low relative magnetic susceptibility.*

ZMNS059A

According to the modelling the thickness of NS059A varies between 50–100 m in the two modelled profiles (Figures 5-30 to 5-31). The modelled dip is slightly towards west.

NS001

The modelling of NS001 indicates an almost vertical dip with only a slight inclination towards west (Figure 5-32).

The forward modelling of magnetic data has many degrees of freedom and a fairly large part of the fit to measured data is achieved by adjusting the near-surface part of the model bodies. The deeper parts of the bodies are not as well constrained. This means that the interpreted dips might reflect near-surface geometry even though the models extend to depths of several hundred meters.

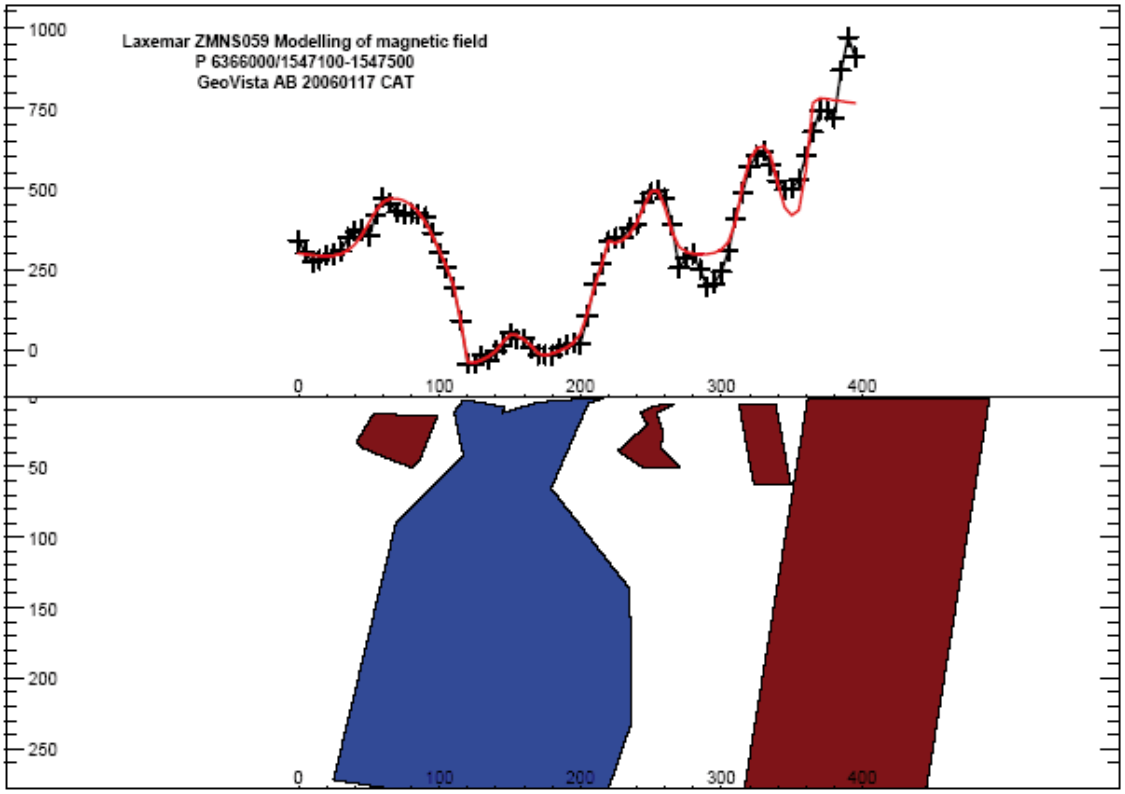

Figure 5-30. *Forward modelling of magnetic total field data over ZMNS059A (profile NS059-1). East is towards right in the figure. Blue bodies have low relative magnetic susceptibility.*

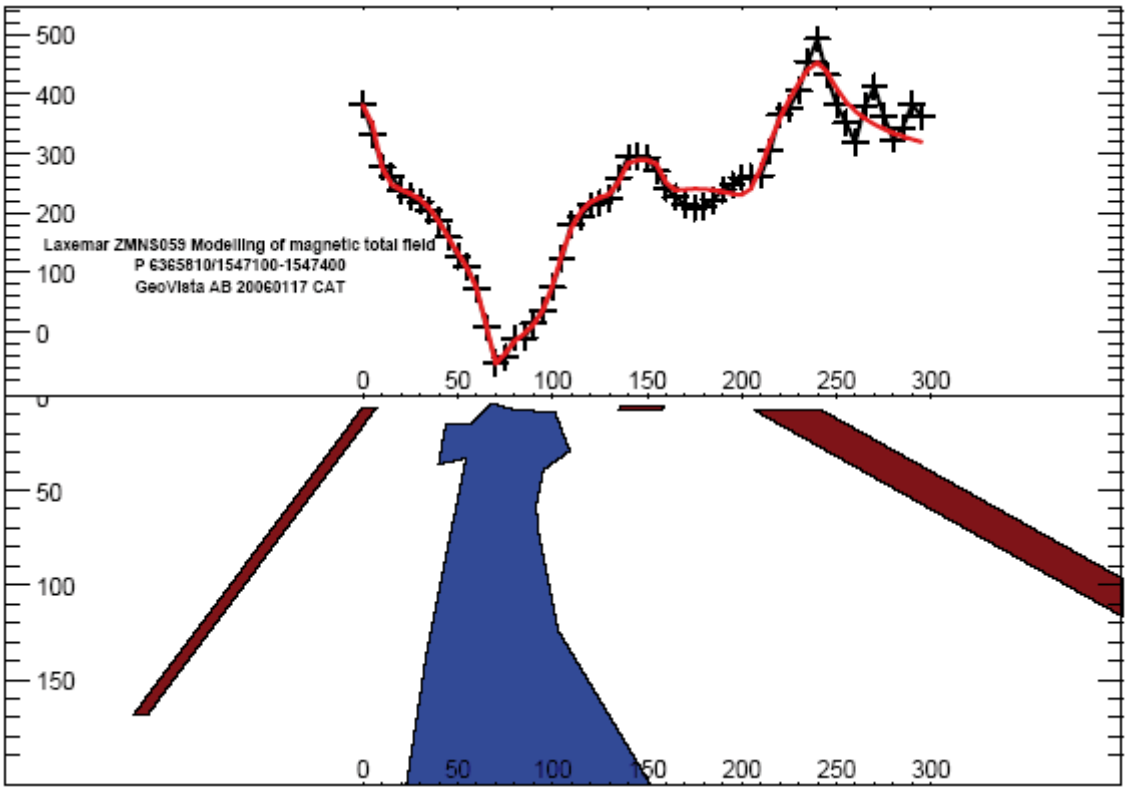

Figure 5-31. *Forward modelling of magnetic total field data over ZMNS059A (profile NS059-2). East is towards right in the figure. Blue bodies have low relative magnetic susceptibility.*

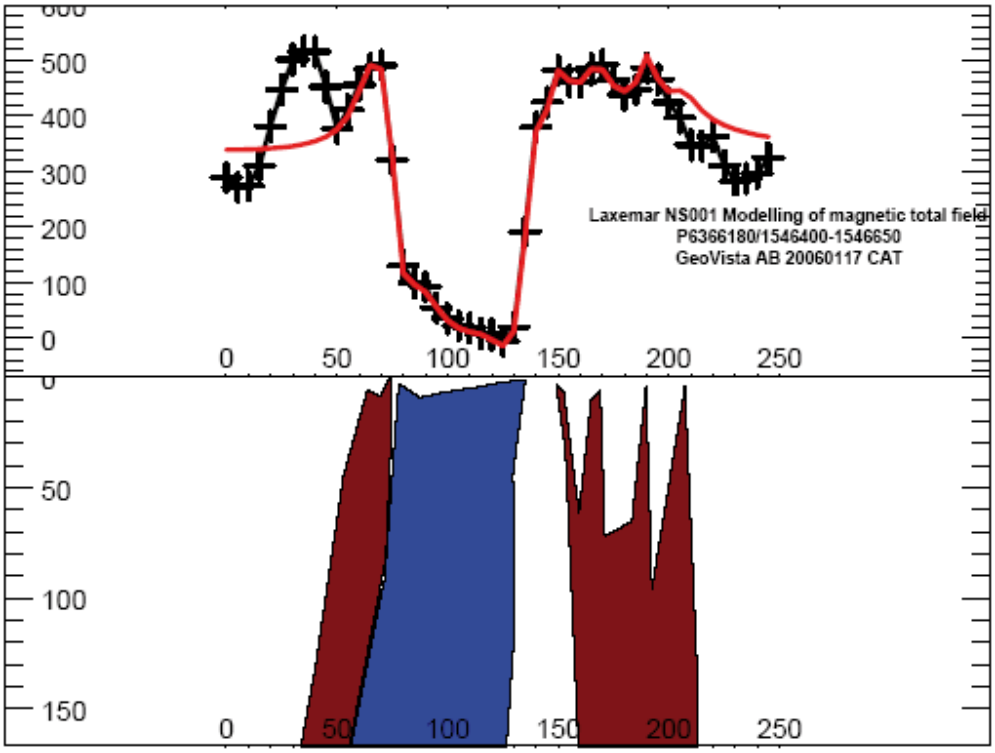

Figure 5-32. *Forward modelling of magnetic total field data over NS001 (profile NS001-1. East is towards right in the figure. Blue bodies have low relative magnetic susceptibility.*

5.5 2D-inversion of resistivity data

The resistivity data were entered, one profile at a time, into the program RES2DINV.
The program uses a model consisting of a regular net of prisms that have an infinite length perpendicular to the profile. The prisms are arranged in such a way that the topography along the profile is mimicked. The resistivity of each prism is iteratively adjusted until a satisfactory fit between the model response and the measured data is achieved. Since there is no unique solution to the problem, the perturbation of the model is constrained by smoothness for each iteration. This prevents unrealistic oscillations of resistivity between neighbouring cells in the model. Since the assumption of two-dimensional geometry often is not satisfied, the model can sometimes contain artefacts due to structures to the side of the profile.

The inversions were carried out with a low value for the vertical/horizontal smoothness filter and with the robust inversion constraint (see Section 4.4.2).

The two-dimensional inversion is generally more sensitive to local anomalies compared to the three-dimensional inversion. Some of the weak bedrock anomalies that were observed in two-dimensional sections were smeared out in the more conservative three-dimensional inversion.

Examples of inversion results can bee seen in Figures 5-33 to 5-36.

Figure 5-33 shows the inverted results for profile 6365500N (cf Figure 5-7) in the eastern survey area (Figure 1-1). The (dark) bluish colours corresponding to low resistivity near the surface are due to the soil cover, which in general is quite thin along this profile. In particular, an area with low-resistive cover appears between 1549050E and 1549100E. This cover has a great influence on the pseudo-section in Figure 5-7 and hence in the depth-slices in Figure 5-4. Only one obvious low-resistivity bedrock anomaly appears in Figure 5-33 at 1549050E. The position of the anomaly fits well with the doubtful southern continuation of NS046 although the relation is not that clear if other profiles are considered (see Section 5.7 below). The dip of the structure seems to be towards west but it is not well determined.

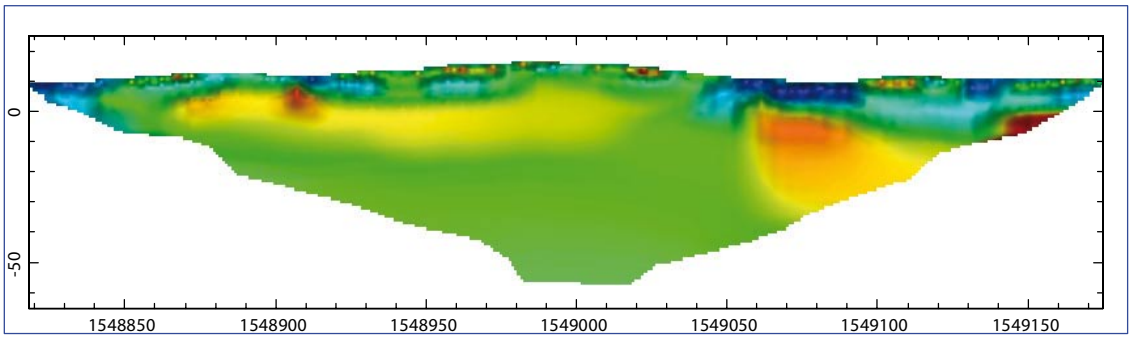

Figure 5-33. *Inverted section 6365500N from the eastern survey area. The low-resistive anomaly at 1549050E is at the position of the previously identified lineament NS046.*

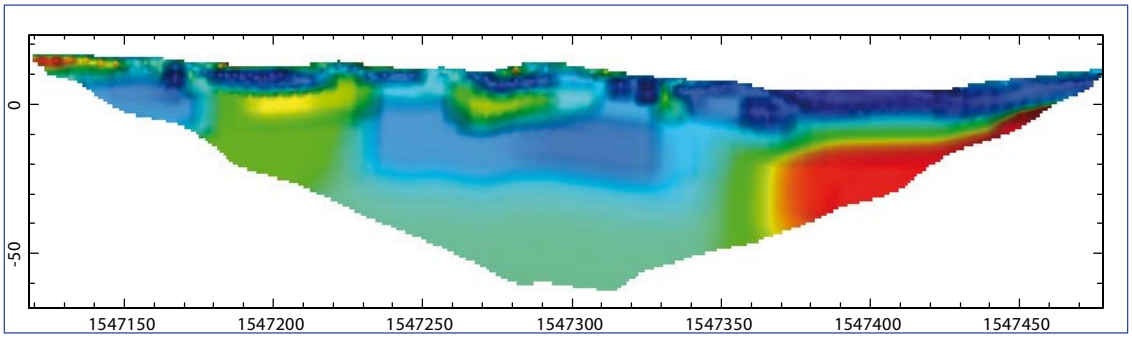

Figure 5-34. *Inverted section 6366050N from the central survey area. The low-resistive anomaly at 1547245E is at the position of NS059.*

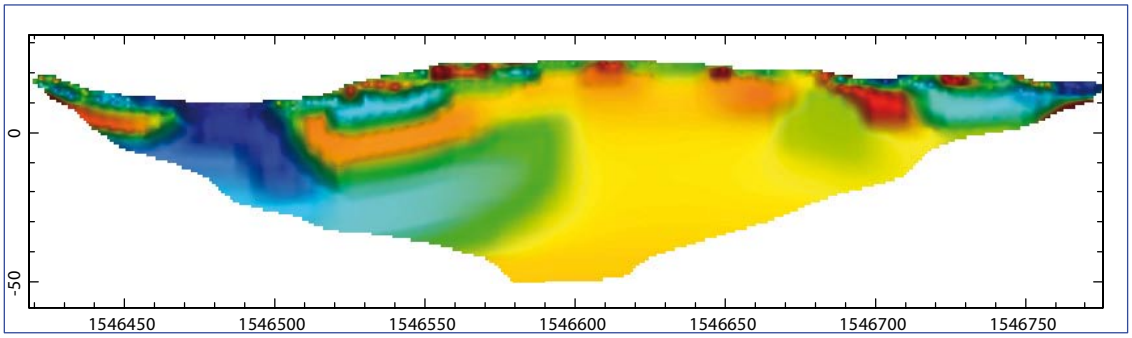

Figure 5-35. *Inverted section 6366390N from the western survey area. The low-resistive anomaly at 1546480E is at the position of NS001.*

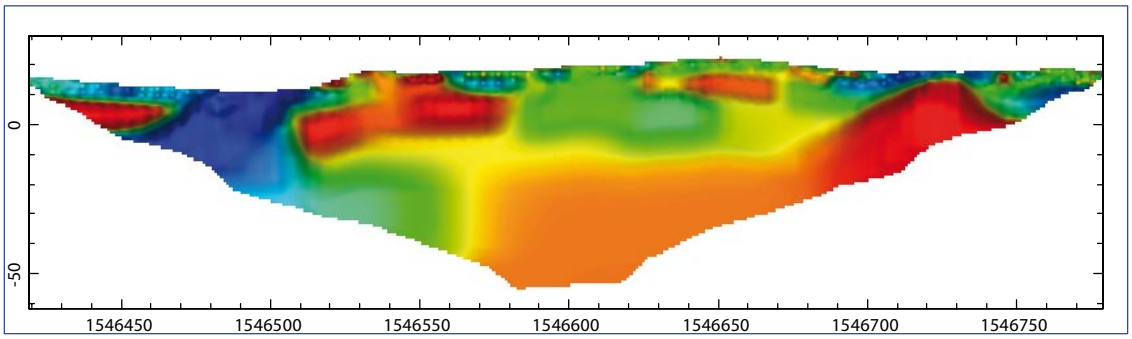

Figure 5-36. *Inverted section 6366500N from the western survey area. The low-resistive anomaly at 1546480E is at the position of NS001. NS001 appears to be dipping to the west.*

Figure 5-34 shows an inverted section for the profile 6366050N in the central survey area (Figure 1-1). A quite wide area of low resistivity appears in the central part of the section. The width of this area is about 120 m. The position of NS059 is at 1547245E which corresponds to the westernmost part of the low-resistive area. It should be pointed out that the resolution of the resistivity inversion is quite limited at large depths and that it is quite possible that the low-resistive area consists of several narrower features with rock of higher resistivity in-between. Even though not obvious in Figure 5-34, it seems as the anomaly corresponding to NS059 dips to the west.

The inverted section of profile 6366390N from the western survey area (Figure 1-1) crosses NS001 at around 1546485E (Figure 5-35). A distinct low-resistivity anomaly can be seen in the inverted section at this position. The resistivity is so low that no clear border to the soil cover can be seen. A gently dipping, near-surface feature can be seen to the east of NS001. It reaches the surface at approximately 1546580E. This feature can be found at several nearby profiles and it is therefore likely that it corresponds to a true bedrock anomaly. The soil cover is very thin or absent in this part of the profile. Several such features, gently dipping to the west can be seen in this area. NS001 appears to be dipping to the east in Figure 5-35. However, most profiles indicate a westerly dip of this feature, like e.g. profile 6366500N (Figure 5-36). Contrary to NS059, the host rock to NS001 has high resistivity.

5.6 3D-inversion of resistivity data

The resistivity profile data were bundled into three large data files, one for each survey area and entered into the program RES3DINV. The survey is not truly three-dimensional since measurements have been done along profiles in one direction only. However, three-dimensional inversion will take into account the effect of resistivity anomalies to the side of a profile and some artefacts in the inversion results will thus be avoided. Three-dimensional inversion tends to be more conservative compared to two-dimensional inversion. Some of the minor local anomalies that appear in two-dimensional results might therefore get smeared out in the three-dimensional model.

The three-dimensional inversion results for the eastern area (Figure 1-1) can be seen as three depth slices in Figure 5-37. The rather low resistivity in the northern and central part of the shallowest slice is due to water-saturated soil cover. The two deeper slices indicates high bulk resistivity in the area. The low-resistivity anomaly slightly to the west of the map centre coincides with the drill site for KLX05 and is probably due to interference from man-made objects. The low resistivity in the south-east corner is an inversion artefact due to clayey soil cover to the south of the survey area. No linear low-resistivity structure is significant enough to produce a continuous anomaly through the deepest slice shown in Figure 5-37.

The three-dimensional inversion results for the central survey area (Figure 1-1) can be seen in Figure 5-38 as depth slices. The low resistivity seen in the shallowest slice indicates that most of the area is soil covered and quite large areas are covered by clayey soil (dark blue in the slice). NS059 shows up as a low-resistivity semi-linear feature in the deeper slices. However, two other shorter structures, striking SSW-NNE give more distinct anomalies.

The three-dimensional inversion results for the western survey area (Figure 1-1) can be seen in Figure 5-39 as depth slices. The shallowest slice indicates that, except for two narrow valleys, most of the area has no or very thin soil cover. NS001 shows up as a distinct linear anomaly for all slices. The area is characterized by a fairly large number of NS-trending features. The resistivity, apart from NS001, is quite high for the deepest slice.

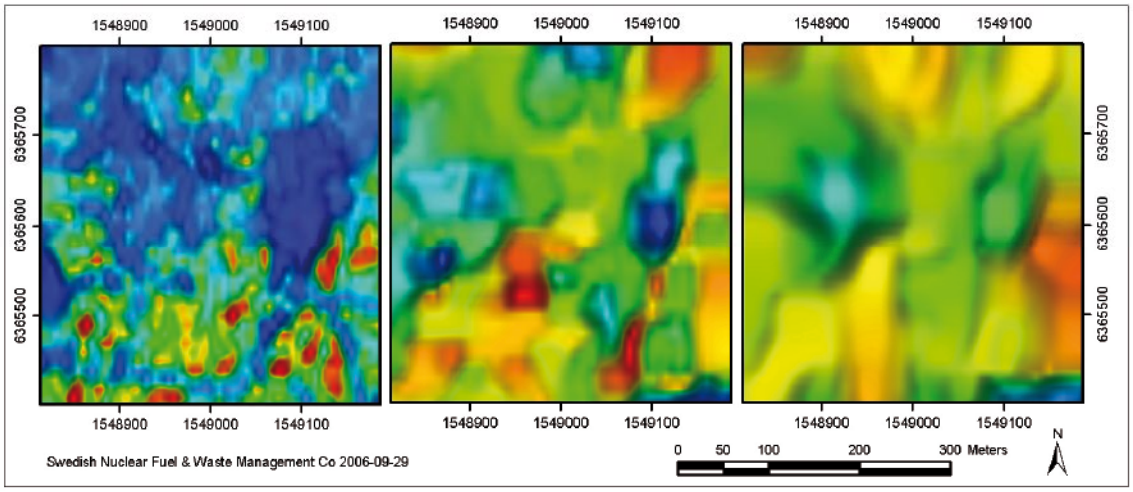

Figure 5-37. *Depth slices of inverted resistivity data from the eastern survey area. The model depths are: 4.2 m (left), 15.6 m (centre) and 33 m (right).*

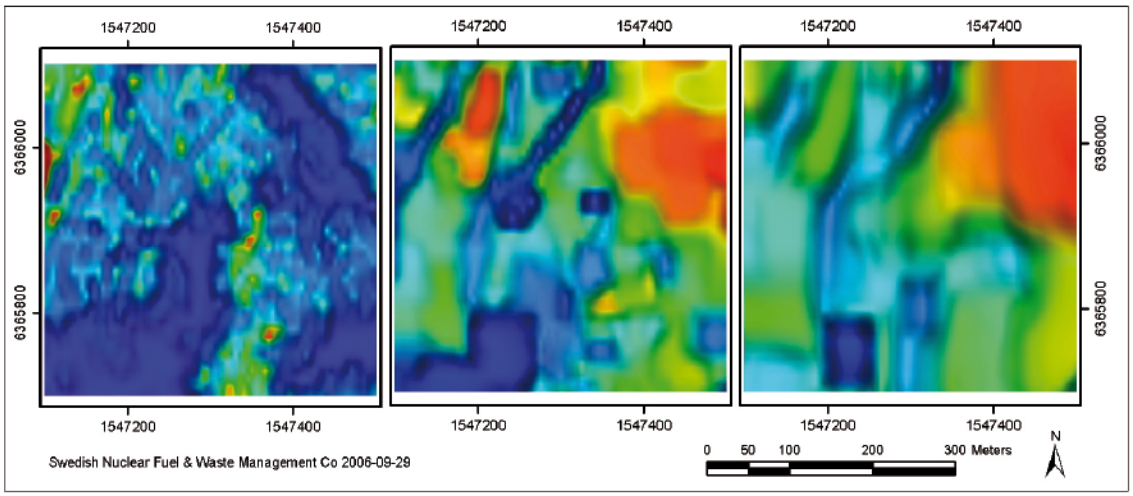

Figure 5-38. *Depth slices of inverted resistivity data from the central survey area. The model depths are: 4.2 m (left), 15.6 m (centre) and 33 m (right).*

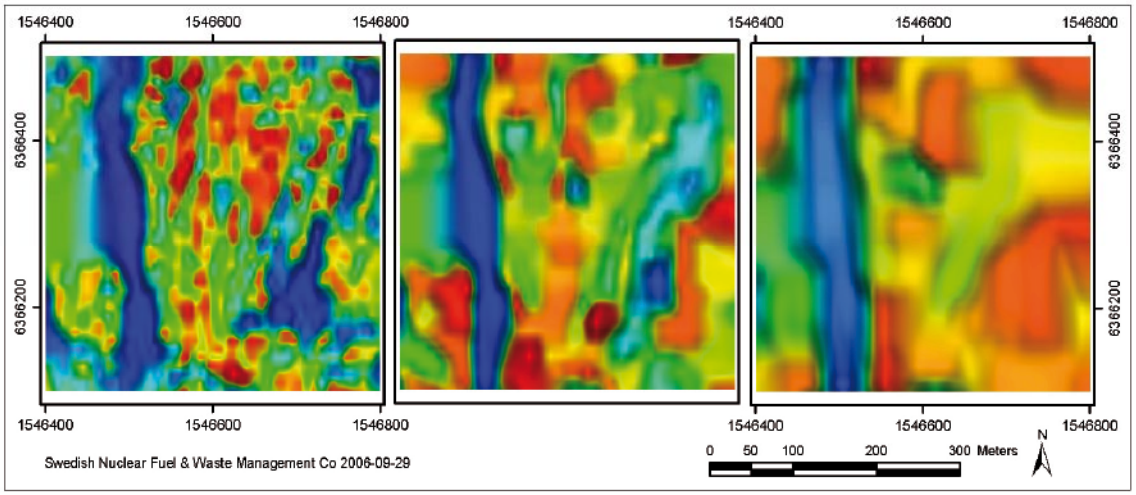

Figure 5-39. *Depth slices of inverted resistivity data from the western survey area. The model depths are: 4.2 m (left), 15.6 m (centre) and 33 m (right).*

5.7 Identification of lineaments in resistivity data

Lineaments in the resistivity data were identified in a process of joint interpretation of inverted two-dimensional sections and depth-slices from the inverted three-dimensional models. The apparent resistivity maps were also used although with some care since they are greatly affected by clayey soil cover. Bedrock anomalies were identified in the two-dimensional results and plotted as symbols at corresponding position in a map. The positions of these symbols were compared with low-resistivity linear trends in the three-dimensional slices. Shallow slices mainly indicate zones of increased soil cover thickness whereas deep slices show true bedrock resistivity anomalies. The dips of the structures were interpreted from the two-dimensional sections and where reliable dip estimates have been identified they are marked in the figures below.

Figure 5-40 shows interpreted lineaments for the eastern survey area (Figure 1-1). As was pointed out in Sections 5.5 and 5.6 no major bedrock resistivity anomalies have been found in this area. The NS- trending structure at easting 1549070 corresponds to the position of the previously identified lineament NS046. It is however a weak and rather discontinuous structure in the resistivity data.

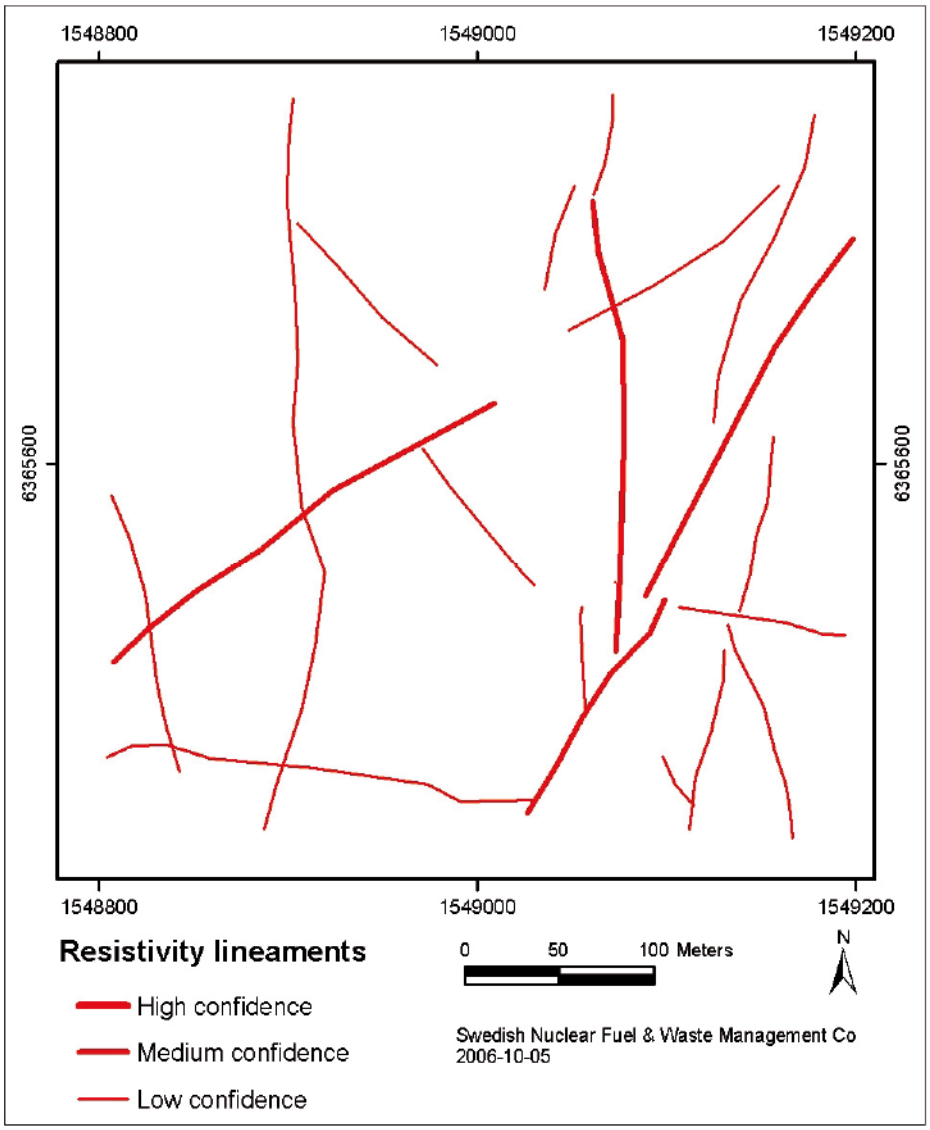

Figure 5-40. *Interpreted resistivity lineaments from the eastern survey area.*

The central survey area is characterized by several short but rather distinct resistivity anomalies trending NNE-SSW (Figure 5-41). They appear in a wide zone of fairly low bulk resistivity. Most of them appear to be dipping to the west although one is dipping towards east. A NS-trending but not completely continuous structure coincides with NS059. This structure also shows a dip towards west.

Most of the western survey area has a very thin soil cover. This means that the ability of the method to detect weak resistivity bedrock anomalies is enhanced. The density of lineaments is therefore higher in this area compared to the other two (Figure 5-42). The area is characterized by NS- trending structures, parallel to NS001. Several of these structures seem to have a gentle dip towards west. NS001 shows up as a distinct lineament also dipping to the west. The dip angle is not possible to estimate since the structure is located outside the area of maximum depth coverage of the survey. The dip of NS001 however seems to be steeper compared to the minor structures to the east.

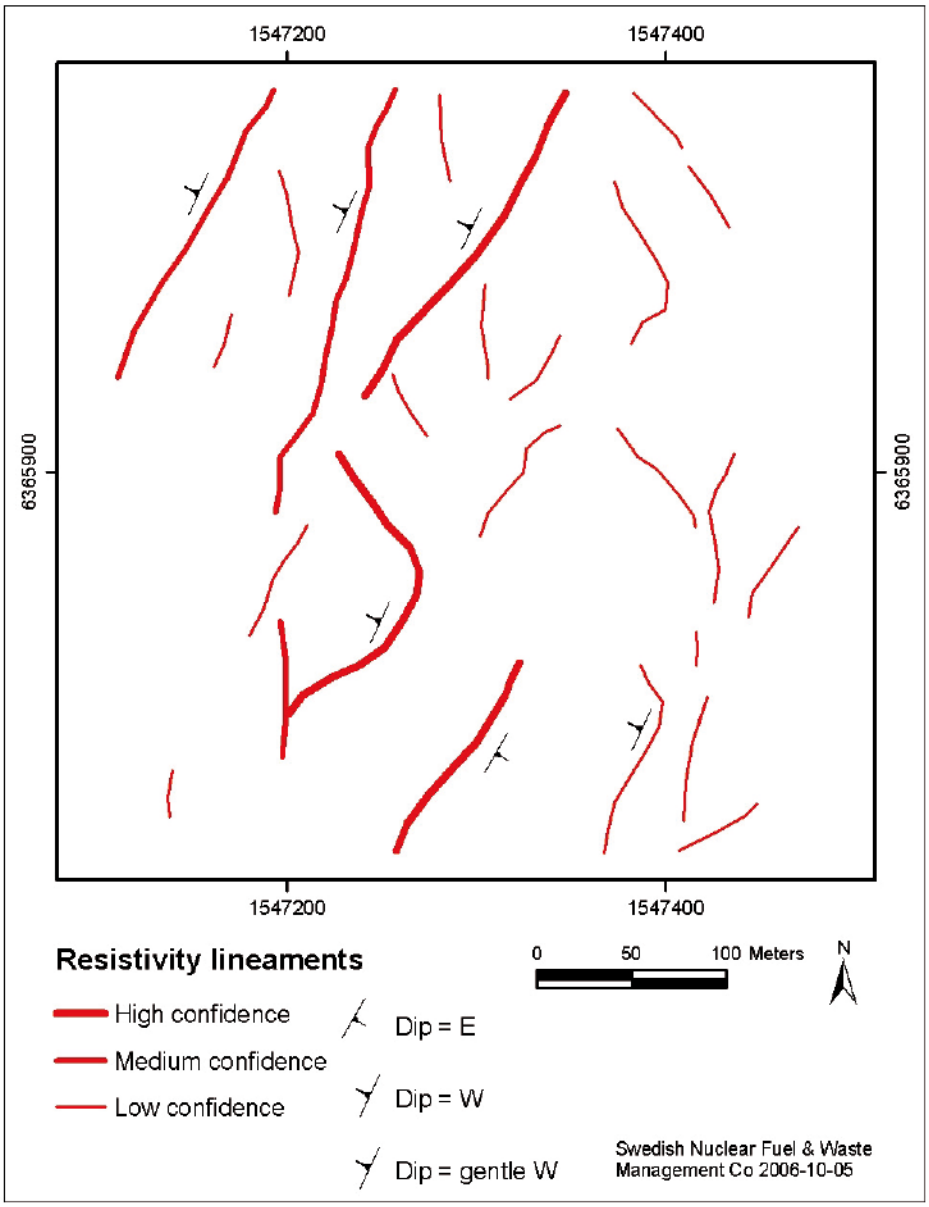

Figure 5-41. *Interpreted resistivity lineaments from the central survey area. Line thickness indicate the confidence of the respective lineaments. Symbols indicate interpreted dip where reliable estimates have been possible to make*

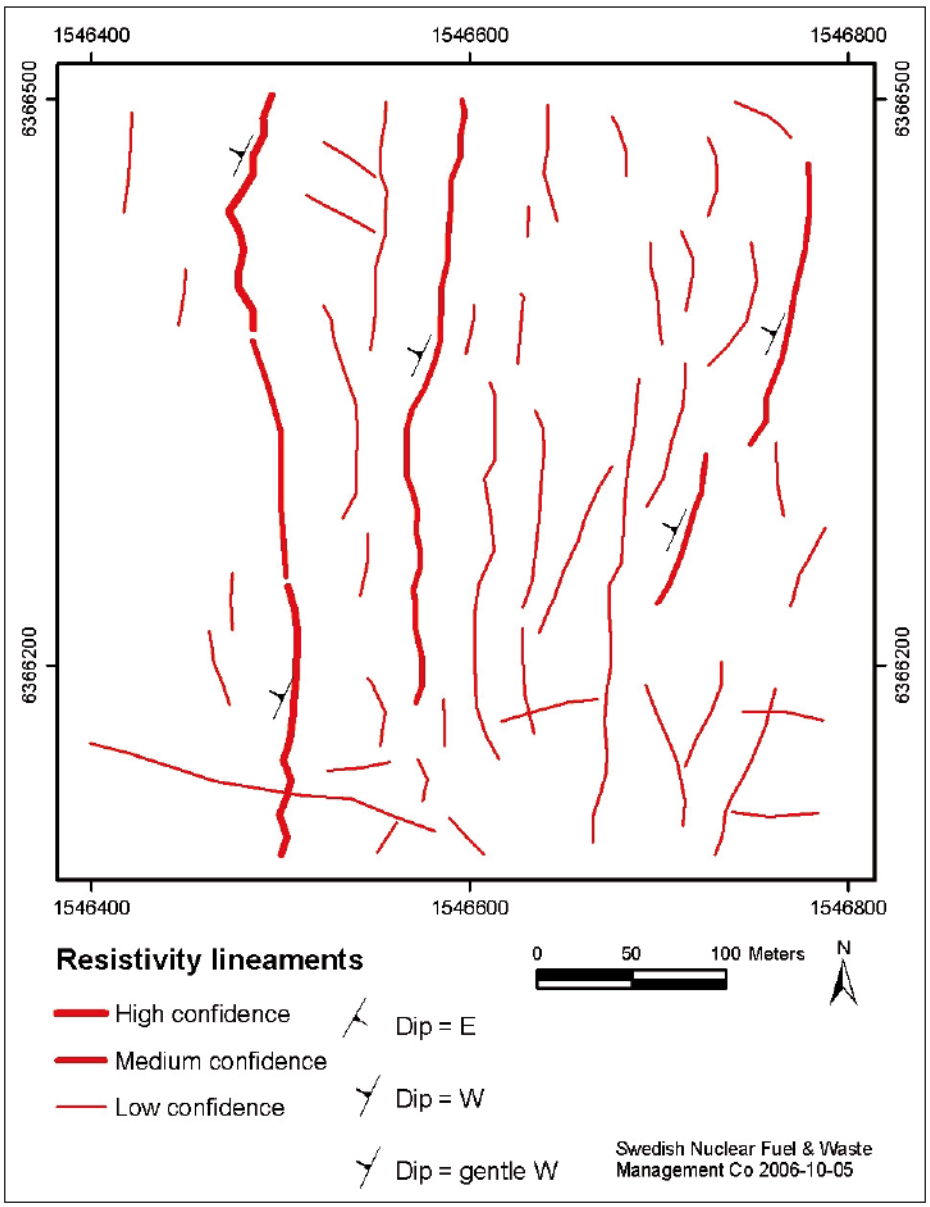

Figure 5-42. *Interpreted resistivity lineaments from the western survey area. Line thickness indicate the confidence of the respective lineaments. Symbols indicate interpreted dip where reliable estimates have been possible to make. The thick line at easting1546500 corresponds to NS001.*

5.8 Interpretation of soil cover thickness and soil units from resistivity data

The soil cover thickness has been interpreted from the inverted resistivity sections. The electrode separation of 5 m does not provide data to accurately resolve soil cover thinner than around one to two metres.

The soil cover at Laxemar is dominated by a sandy moraine /11/. The resistivity of this moraine has been estimated with resistivity soundings /12/ and is relatively high, 1,000 to 1,500 Ωm in water saturated volumes and considerably higher in non-saturated volumes. These values are comparable to the resistivity of fractured rock. It is therefore difficult to interpret the soil-rock interface at the locations of suspected deformation zones or generally increased fracturing.

Clayey soils appear at some locations, especially in valleys /11/. The resistivity of these soils is low /12/, around 50 Ωm. It is therefore difficult to see if the clayey soils are deposited on moraine or more or less directly on the bedrock. It is therefore possible that the soil cover thickness has been under-estimated at some places covered by clayey soils.

The estimation of soil cover thickness from resistivity data is affected by the principle of resitivity equivalence. Also, the type of inversion performed with the data provides more or less smooth transitions between different units. This has the effect that the interpreted soil cover thickness is overestimated. The interpreted soil cover thickness was therefore compared with results from refraction seismic profiles /14, 15/. Figure 5-43 shows the relation between soil cover thickness interpreted from this resistivity survey and from a refraction seismic profile from the central area. There is a quite good correlation even though the slope of the fitted line is not equal to 1.0. The estimates from the resistivity surveys were therefore adjusted in accordance with the regression value from Figure 5-43.

Figure 5-44 shows the estimated soil cover thickness for the eastern survey area. The limited depth coverage at each end of the profiles prevents any estimates. The area is characterized by a soil cover of, in general, four to six metres in the northern half and less than 2 m in the southern half. The soil cover thickness was subtracted from an elevation model based on LIDAR data /16/, providing a map of the bedrock relief (Figure 5-44).

The results above for the eastern area were based on the three-dimensional inversion results. The three-dimensional inversion did however not provide a good base for soil cover thickness estimates for the other two areas. Instead, the results from two-dimensional inverted sections were used. Those sections might be affected by e.g. variations in soil cover thickness perpendicular to the profile. The end-result of this is that the maps appear a bit stripy in the direction of the profiles.

The estimated soil cover thickness and bedrock relief for the central and western survey areas can be seen in Figures 5-45 and 5-46 respectively. It should be noted that the resistivity in NS001 is of the same order as in the overlying soil and that the soil-rock interface was very difficult to interpret.

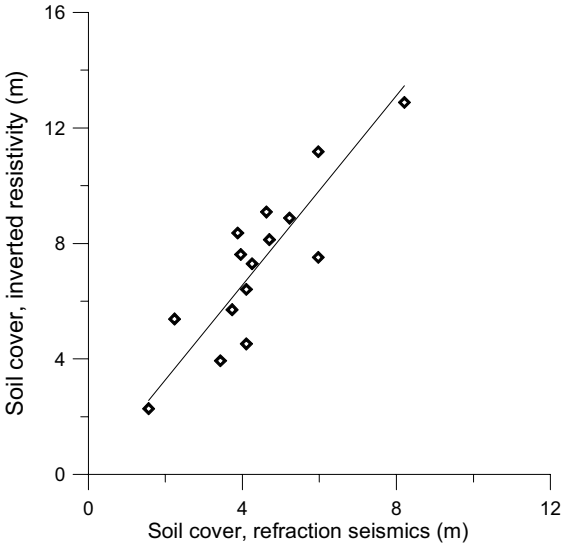

Figure 5-43. *Estimated soil cover thickness from resistivity and refraction seismics at the same positions. The straight line is a fitted line through the origin with a slope of 1.64. The resistivity depth estimates was later adjusted with this value.*

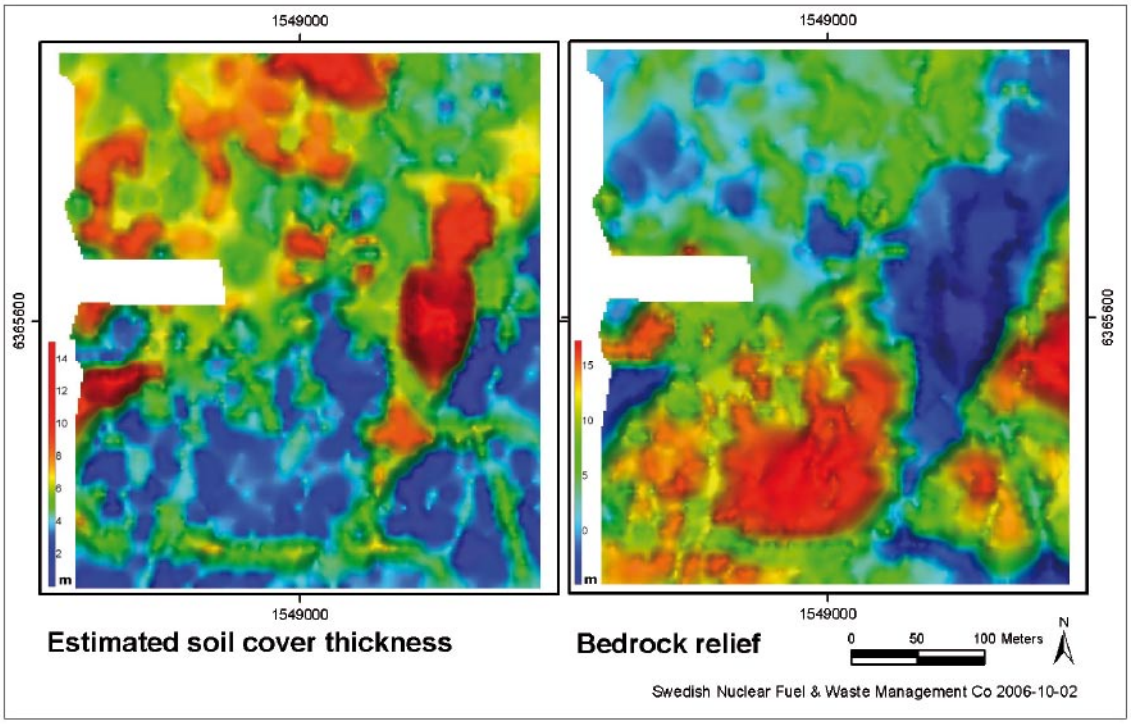

Figure 5-44. *Estimated soil cover thickness for the eastern survey area (left). The values have been linearly adjusted after comparisons with refraction seismic results. The resulting bedrock relief is shown to the right.*

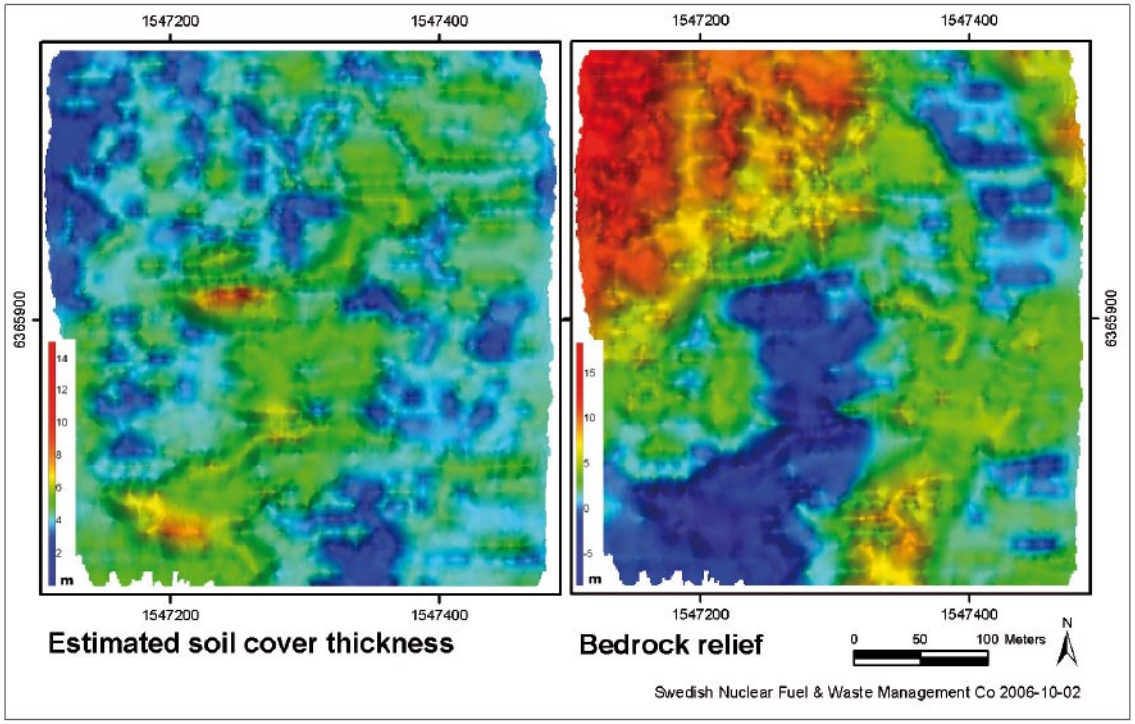

Figure 5-45. *Estimated soil cover thickness for the central survey area (left). The values have been linearly adjusted after comparisons with refraction seismic results. The resulting bedrock relief is shown to the right.*

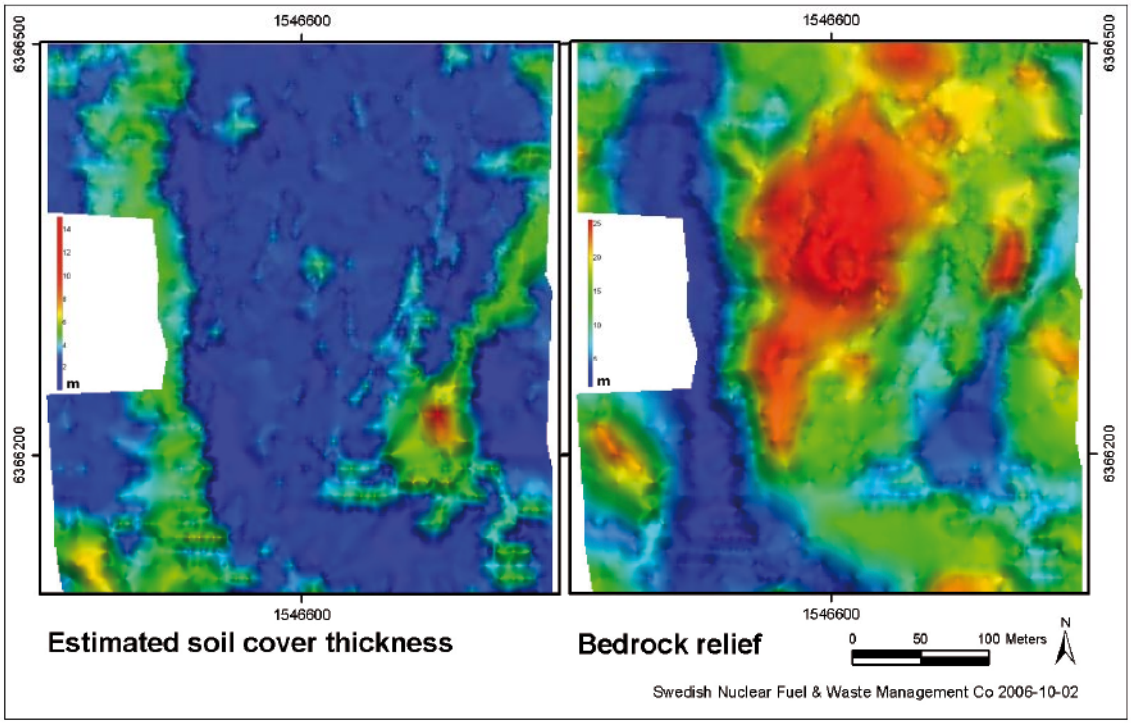

Figure 5-46. *Estimated soil cover thickness for the western survey area (left). The values have been linearly adjusted after comparisons with refraction seismic results. The resulting bedrock relief is shown to the right.*

Soil units with resistivities compatible with the resistivity determined for clayey soils /12/ in the area have been identified (Figures 5-47 to 5-49). Very thin clayey soil cover will not be resolved by the method. The identified areas will therefore correspond to areas with a clayey cover of at least around 1 m.

Areas with very thin soil cover (less than 1 to 2 m) have also been marked in Figures 5-47 to 5-49. It should however be pointed out that non-saturated moraine might have a resistivity comparable to fresh bedrock. Such moraine cover might therefore be missed.

5.9 Bulk resistivity

The overall resistivity or bulk resistivity of the rock mass is affected by the fracturing, porosity and alteration of the rock. It can therefore be seen as an indicator of the quality of the rock. The bulk resistivity is also affected by the salinity of the pore water. However, we can assume that the depth of investigation is small enough not to be affected by saline ground water.

The apparent resistivity measurements are affected by the clayey soil-cover. The effect of the soil cover can be neglected if the separation between the electrodes is large enough. Histograms for the apparent resistivities measured with 400 m between the two current electrodes (the largest separation used) can be seen in Figure 5-50. All three areas have peaks in the histograms at values larger than 5,000 Ωm. This can be considered as rather high values for the bulk resistivity. However, the central area has its peak at a lower value compared to the other two areas.

Another way to compare bulk resistivities is to use the inverted resistivity for a depth larger than the largest expected soil cover thickness in the area. Figure 5-51 shows histograms for the resistivity at 33 m depth from the three-dimensional inversions of the resistivity data. These results should, in theory, be unaffected by soil cover thinner than 33 m. The eastern and western areas have major peaks at around 30,000 Ωm, which can be considered as very high values.

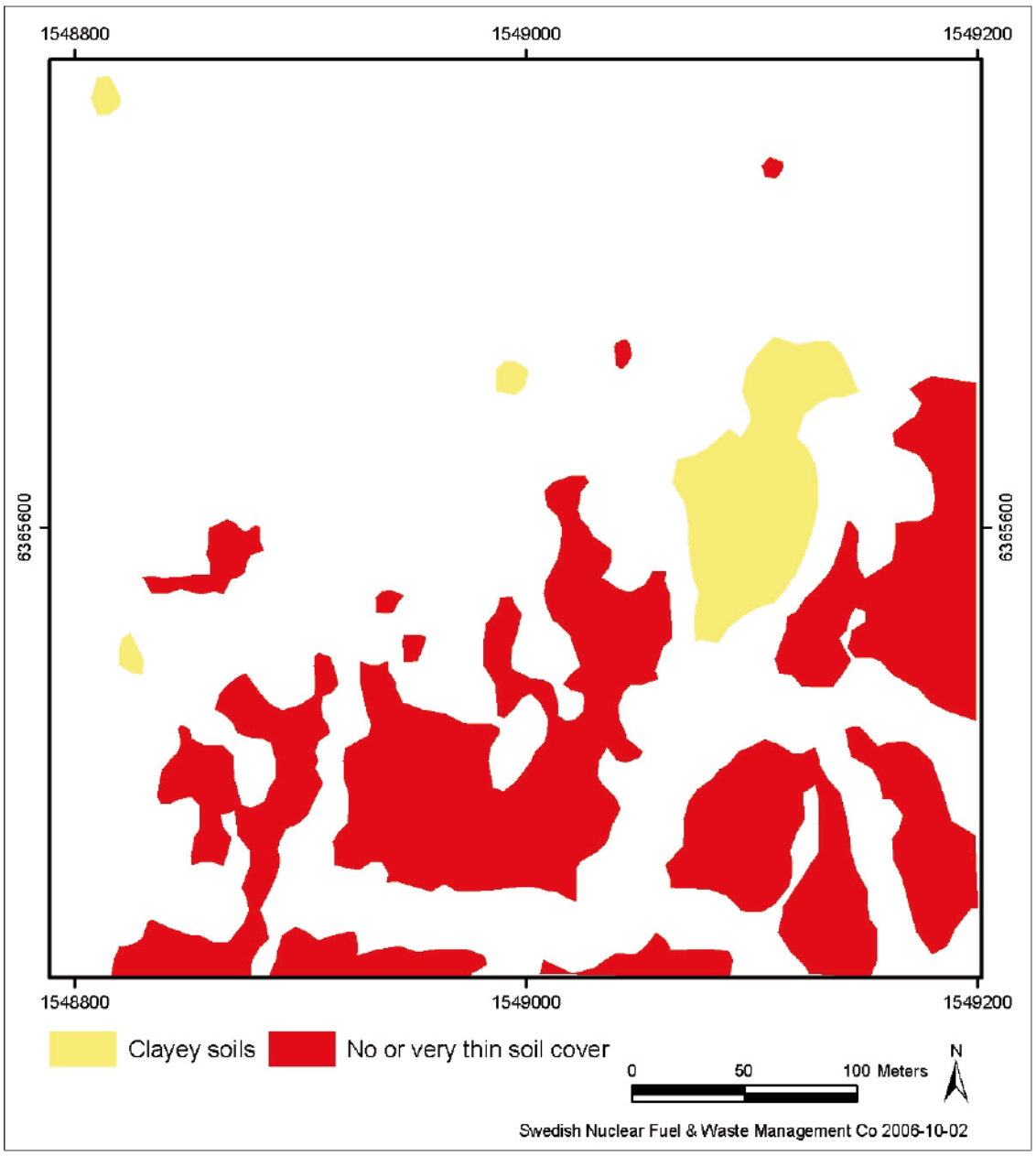

Figure 5-47. *Estimated soil cover for the eastern survey area. Yellow areas are interpreted to be covered by clayey soils. Cover of less that around 1 m might not be resolved by the method. Red areas are interpreted to have no or very thin soil cover.*

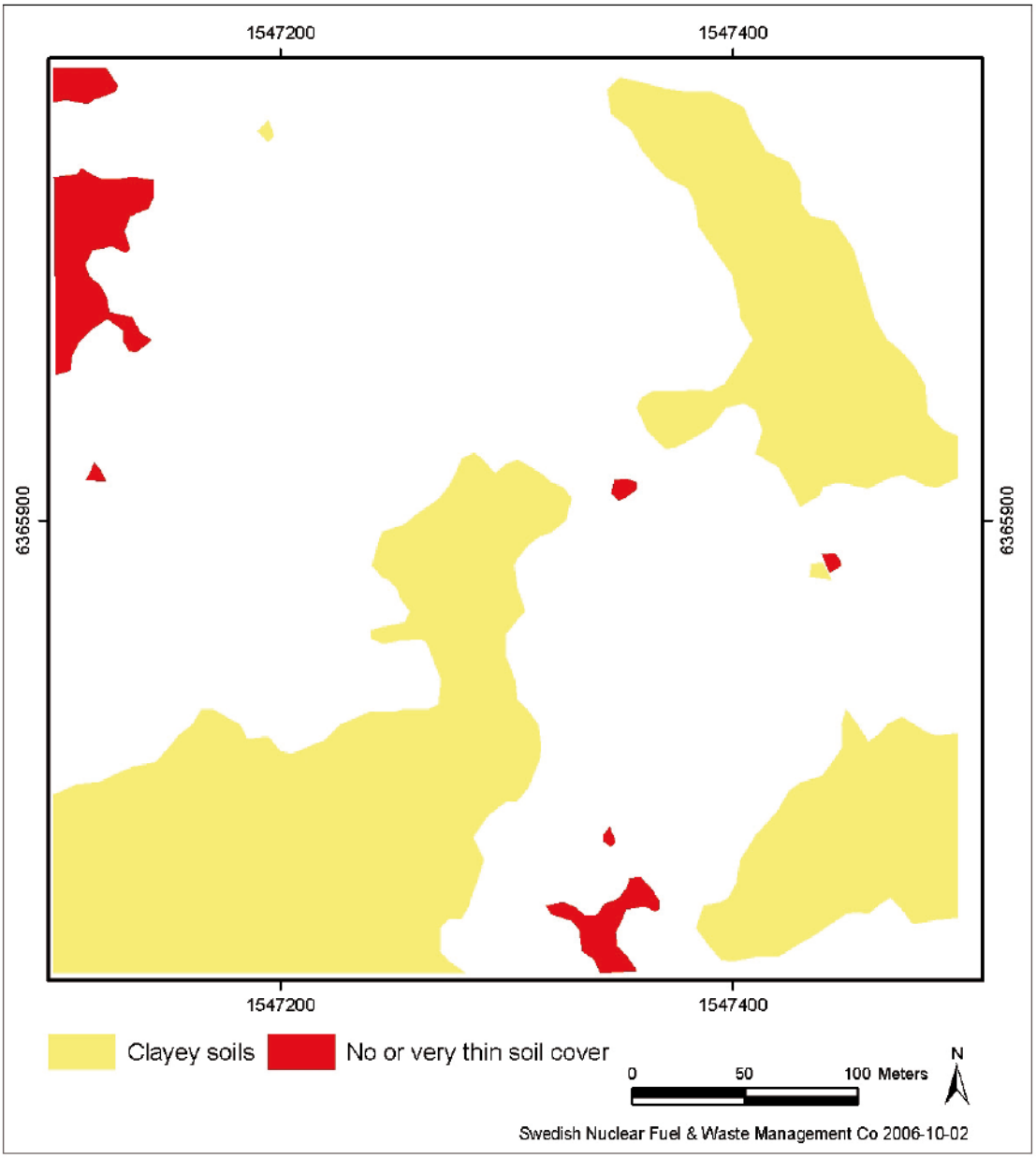

Figure 5-48. *Estimated soil cover for the central survey area. Yellow areas are interpreted to be covered by clayey soils. Cover of less that around 1 m might not be resolved by the method. Red areas are interpreted to have no or very thin soil cover.*

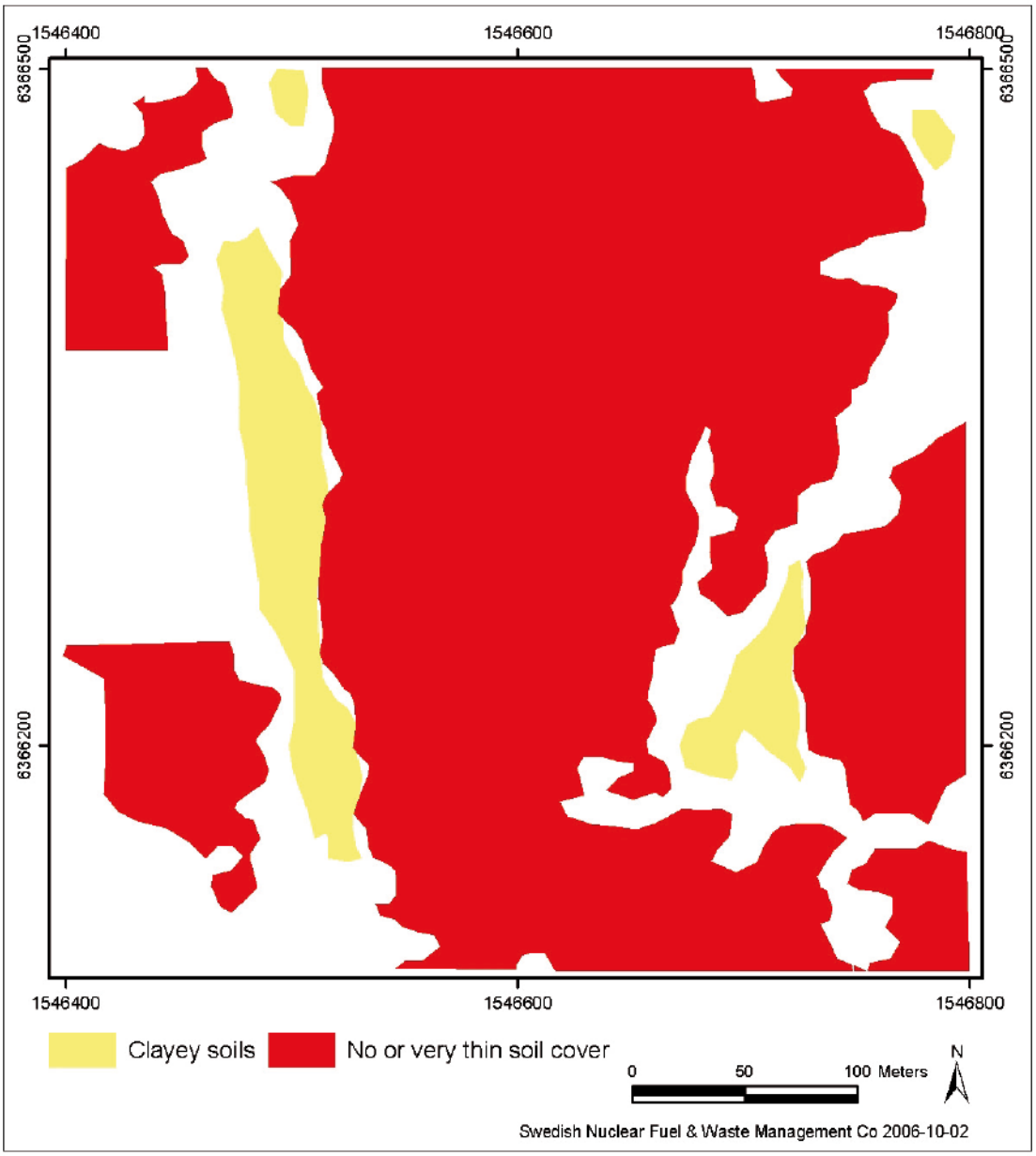

Figure 5-49. *Estimated soil cover for the western survey area. Yellow areas are interpreted to be covered by clayey soils. Cover of less that around 1 m might not be resolved by the method. Red areas are interpreted to have no or very thin soil cover.*

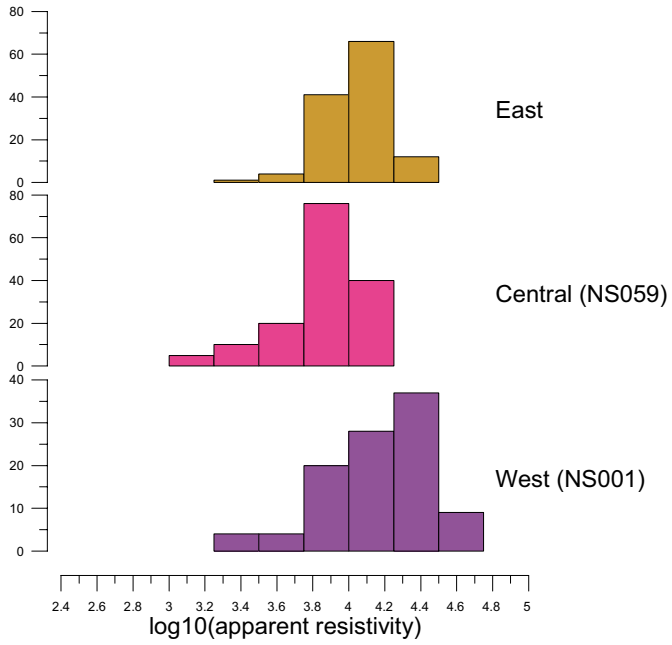

Figure 5-50. *Histograms for apparent resistivities measured with a distance between the current electrodes of 400 m.*

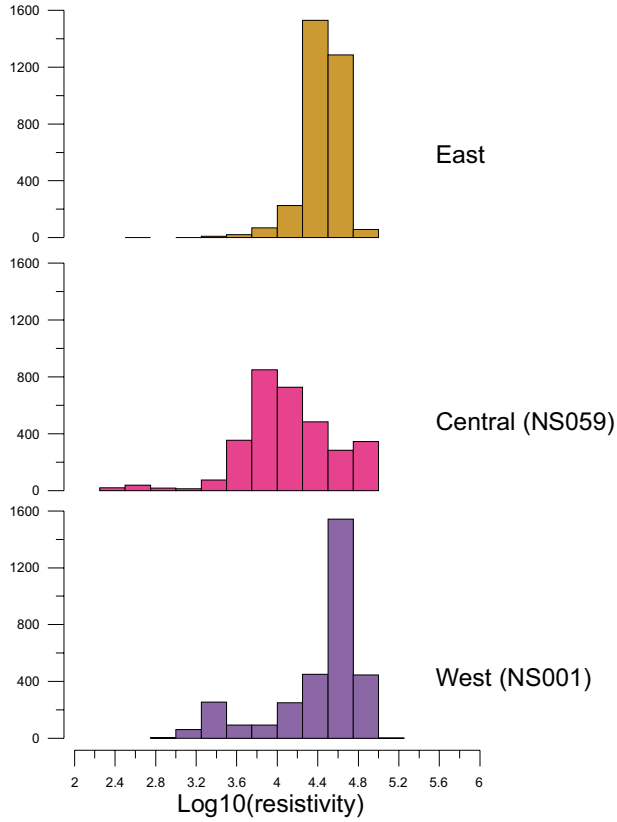

Figure 5-51. *Histograms for inverted resistivities at a model depth of 33 m.*

The minor peak at around 2,500 Ωm for the western area is due to model blocks affected by NS001. The peak in the histogram is at a significantly lower value for the central area compared to the major peaks for the other two areas. The median value for model resistivities at this depth is around 0.4 to 0.5 orders of magnitude lower for the central area than for the other two areas. This can be translated to fracture parameters or porosity with different empirical models. According to the model of Stesky /17/ the difference would correspond to 2.5 to 3 times higher fracture frequency or average fracture aperture. According to Archie's law /18/ the difference would correspond to 1.7 to 1.9 times higher porosity.

5.10 High magnetic lithological in-homogeneities

According to petrophysical studies /1, 2, 3/ the magnetisation of the diorite/gabbro is often higher compared to the Ävrö-granite and to the quartz monzodiorite. The fine-grained dioritoid has a very broad distribution in the frequency diagram of the magnetic susceptibility where some measurements show very high magnetic susceptibilities. In areas with high magnetisation levels it could thus be expected that diorite/gabbro, or the high susceptibility forms of the fine-grained dioritoid, would more often be observed as compared to areas with a normal magnetisation. In a selection process with the aim to isolate such areas a comparison has been made of the magnetic susceptibility measurements on outcrops, the mapping of diorite/gabbro or fine-grained dioritoids, and the total magnetic field as measured in the detailed ground magnetic survey. The selection of areas with high magnetisation with potential presence of diorite/gabbro or fine-grained dioritoid was based on the following criteria:

- a pronounced magnetic high anomaly is selected if no observations of a magnetic susceptibility in either Ävrö-granite or to the quartz monzodiorite higher than $1{,}500\times10^{-5}$ SI is found on or very near the anomaly.

The highly magnetized areas have been compared with the Site Descriptive Model (version 1.2). In Figure 5-52 all indications of highly magnetized rock outside areas marked as diorite/gabbro or fine-grained dioritoids are presented. In Figure 5-52 two different sizes of these areas are distinguished, a comparatively large area is delineated and shown as a green filled area while a small area is represented by a symbol (green circle). The magnetic measurements are disturbed around the power lines and no reliable data have been acquired – these areas are also shown in Figure 5-52.

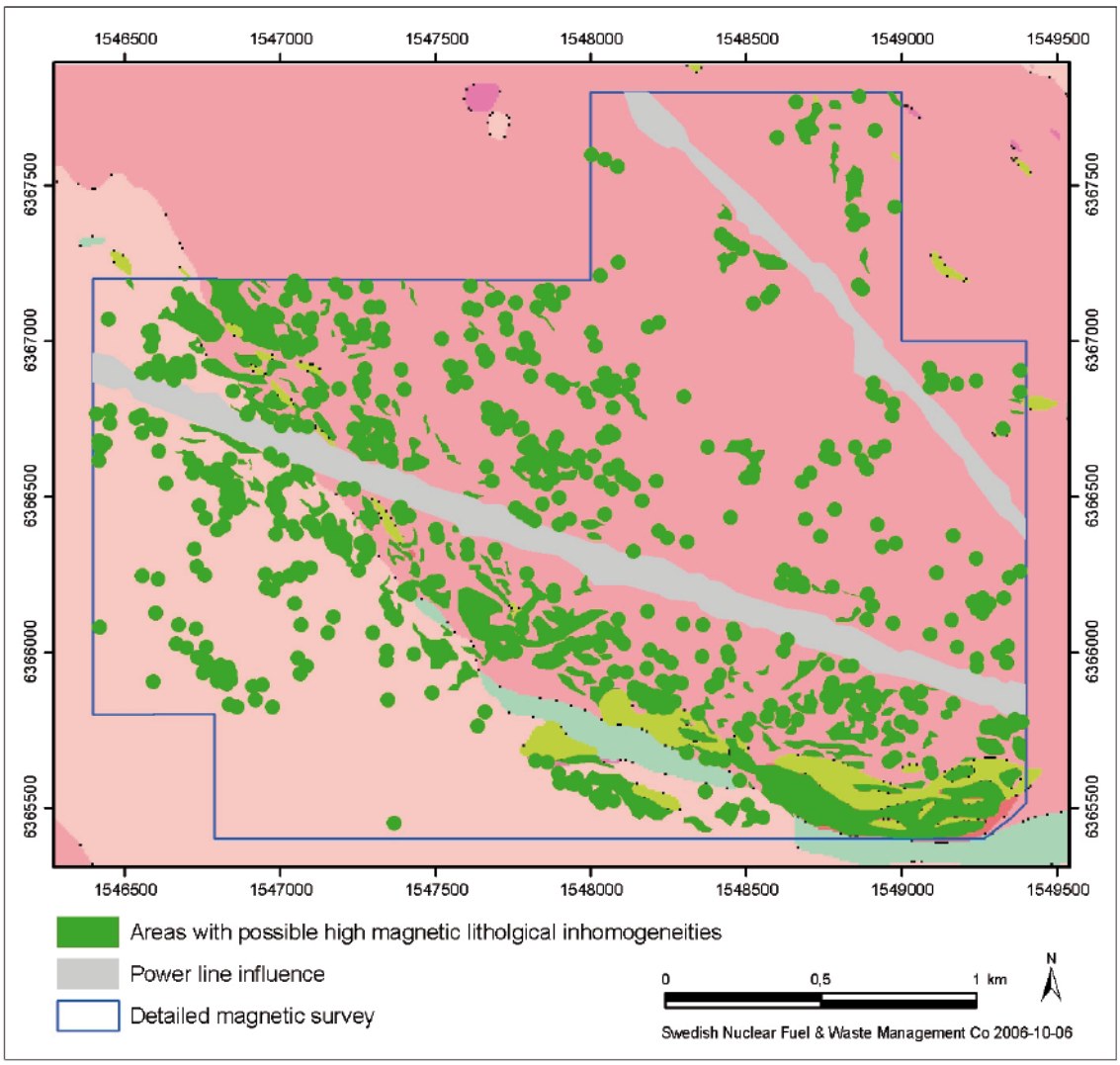

Figure 5-52. *Areas with possible high magnetic lithological inhomogeneities, such as diorite/gabbro or fine-grained dioritoid, are shown in dark green. Areas disturbed by power lines are marked in grey. In the background is shown the geological map from the Site Descriptive Model (version 1.2) over the Laxemar area /19/.*

References

/1/ **Mattsson H, Thunehed H, 2003.** Measurements of petrophysical parameters on rock sample during autumn 2002. SKB P-03-19, Svensk Kärnbränslehantering AB.

/2/ **Mattsson H, Thunehed H, Triumf C-A, 2003.** Compilation of petrophysical data from rock samples and in situ gamma-ray spectrometry measurements. SKB P-03-97, Svensk Kärnbränslehantering AB.

/3/ **Mattsson H, Thunehed H, Triumf C-A, 2005.** Compilation of petrophysical data from rock samples and in situ gamma-ray spectrometry measurements, Stage 2 – 2004 (including 2002). SKB P-04-294, Svensk Kärnbränslehantering AB.

/4/ **Nisca D H, 1988.** Geophysical laboratory measurements on core samples from KLX01, Laxemar and KAS02, Äspö. SKB Progress report 25-88-06, Svensk Kärnbränslehantering AB.

/5/ **Nisca D H, 1987.** Aerogeophysical interpretation bedrock and tectonic analysis. SKB HRL Progress Report 25-87-04, Svensk Kärnbränslehantering AB.

/6/ **Eriksson L, Johansson R, Thunehed H, Triumf C-A, 1997.** Metodtester ytgeofysik 1996. Bestämning av berggrundens bulkresistivitet och djupet till salint grundvatten med halvregional resistivitetsmätning, elektrisk sondering samt transient elektromagnetisk sondering. SKB PR D-98-01, Svensk Kärnbränslehantering AB.

/7/ **Thunehed H, Triumf C-A, Pitkänen T, 2004.** Oskarshamn site investigation. Geophysical profile measurements over interpreted lineaments in the Laxemar area. SKB P-04-211, Svensk Kärnbränslehantering AB.

/8/ **Thunehed H, Triumf C-A, 2005.** Oskarshamn site investigation. Detailed ground geophysical survey at Laxemar. Magnetic total field and resistivity. SKB P-05-188, Svensk Kärnbränslehantering AB.

/9/ **Rönning H J S, Kihle O, Mogaard J O, Walker P, 2003.** Simpevarp site investigation. Helicopter borne geophysics at Simpevarp, Oskarshamn, Sweden. SKB P-03-25, Svensk Kärnbränslehantering AB.

/10/ **Triumf C-A, Thunehed H, Kero L, Persson L, 2003.** Oskarshamn site investigation. Interpretation of airborne geophysical survey data. Helicopterborne survey data of gamma ray spectrometry, magnetics and EM from 2002 and fixed wing airborne survey data of the VLF-field from 1986. SKB P-03-100, Svensk Kärnbränslehantering AB.

/11/ **Rudmark L, Malmberg-Persson K, Mikko H, 2005.** Oskarshamn site investigation. Investigation of Quaternary deposits 2003–2004. SKB P-05-49, Svensk Kärnbränslehantering AB.

/12/ **Thunehed H, Pitkänen T, 2003.** Oskarshamn site investigation. Electrical soundings supporting inversion of helicopterborne EM-data. Primary data and interpretation report. SKB P-03-17, Svensk Kärnbränslehantering AB.

/13/ **Triumf C-A, 2004.** Oskarshamn site investigation. Joint interpretation of lineaments. SKB P-04-49, Svensk Kärnbränslehantering AB.

/14/ **Lindqvist G, 2004.** Oskarshamn site investigation. Refraction seismic measurements in Laxemar. SKB P-04-134, Svensk Kärnbränslehantering AB.

/15/ **Lindqvist G, 2004.** Oskarshamn site investigation. Refraction seismic measurements in Laxemar autumn 2004. SKB P-04-298, Svensk Kärnbränslehantering AB.

/16/ **Nyborg M, 2005.** Oskarshamn site investigation. Aerial photography and airborne laser scanning Laxemar – Simpevarp. SKB P-05-223, Svensk Kärnbränslehantering AB.

/17/ **Stesky R M, 1986.** Electrical conductivity of brine-staurated fractured rock. Geophysics, 51, 1585–1593.

/18/ **Archie G E, 1942.** The electrical resistivity log as an aid in determining some reservoir characterization. Trans. Amer. Inst. Mining and Metal. Eng. vol. 46, pp 54–62.

/19/ **SKB, 2006.** Preliminary site description. Laxemar subarea – version 1.2. SKB R-06-10, Svensk Kärnbränslehantering AB.